View metadata, citation and similar papers at core.ac.uk
brought to you by CORE
provided by Digitale Hochschulschriften der LMU

Effect of temperature and light intensity on the representation of motion information in the fly's visual system

Deusdedit Lineu Spavieri Junior

München 2009

Effect of temperature and light intensity on the representation of motion information in the fly's visual system

Deusdedit Lineu Spavieri Junior

Dissertation zur Erlangung des Doktorgrades der
Naturwissenschaften
an der Fakultät für Biologie
der Ludwig–Maximilians–Universität
München

Angefertigt am Max-Planck-Institut für Neurobiologie
Abteilung Neuronale Informationsverarbeitung

vorgelegt von
Deusdedit Lineu Spavieri Junior
aus Sorocaba-SP, Brasilien

München, den 22.10.2008

Erstgutachter: Alexander Borst
Zweitgutachter: Andreas Herz
Tag der mündlichen Prüfung: 07.04.2009

Contents

1 Summary **1**

2 Introduction **3**
2.1 Motivation . . . 3
2.2 Motion vision overview . . . 6
2.2.1 Phototransduction . . . 6
2.2.2 Retina-Lamina signal transmission . . . 9
2.2.3 Motion detection in the medulla . . . 11
2.2.4 Integration of motion information in the lobula plate . . . 12
2.2.5 H1's outdoor experiments . . . 13
2.3 Goals . . . 15

3 Materials and Methods **17**
3.1 Preparation . . . 17
3.2 Temperature control . . . 18
3.3 Data acquisition and visual stimulation . . . 19
3.4 Data analysis . . . 22
3.4.1 Pre-analysis . . . 22
3.4.2 Information theory . . . 25
3.4.3 Bias correction . . . 28
3.4.4 Classification theory . . . 31
3.4.5 Statistical analysis . . . 32
3.4.6 Temperature and luminance coefficients . . . 33

4 Results **35**
4.1 Extracellular field potentials . . . 36
4.2 Spontaneous firing rate . . . 37
4.3 Stimulus-induced firing rate . . . 39
4.4 Response stationarity . . . 42
4.5 Information rate, encoding window and coding efficiency . . . 44
4.6 Latency . . . 49
4.7 Summary of the results . . . 53

5 Discussion **57**
5.1 Internal and external perturbations 58
5.2 Trade-off between noise and time-scale 58
5.3 Firing rate, spike jitter and information rate 61
5.4 Timing and count encoding modes 62
5.5 Behavioral relevance 63
5.6 Conclusions and outlook 66

List of Figures

2.1 Fly's visual system 8
2.2 Fly's visual system 10
2.3 Objectives of this work 15

3.1 Temperature control 18
3.2 Fly head and H1 anatomy 20
3.3 H1 responses to a time-varying stimulus 23
3.4 Spike count stationarity 24
3.5 Response entrainment to the video refresh rate 25
3.6 Optimal information rate 28
3.7 Bias reduction 30
3.8 Comparison of several bias correction methods 32

4.1 Extracellular potential waveform as a function of temperature 37
4.2 Spontaneous activity as a function of temperature. 38
4.3 Time-varying firing rate 40
4.4 Mean firing rate and precision 42
4.5 Accommodation of spike count 43
4.6 Timing encoding mode - optimal information rate and time scale 45
4.7 Count encoding mode - optimal information rate and time scale 46
4.8 Comparison between count and timing strategies 47
4.9 Entropy rates and firing rate 48
4.10 Response latency 50
4.11 Retinograms 51
4.12 Latency and intensity modulation 53
4.13 Overview 54

5.1 Trade-off between noise and temporal scale 59
5.2 Mutual information between response properties 60
5.3 Optimal encoding window and ISI mode 63
5.4 Body temperature of *Calliphora* during tethered flight. 65

Chapter 1

Summary

To comprehend how the brain performs efficient computation, it is important to understand the way sensory information is represented in the nervous system. Under natural conditions, sensory signals have to be processed with sufficient accuracy under functional and resources constraints.

Here I use motion vision in the fly *Calliphora vicina* to study the influence of two behaviorally relevant environmental properties - temperature and light intensity - on the representation of motion information in the responses of the neuron H1. The goal was to quantify how these environmental properties affect the response variability, information content, coding efficiency and temporal scale.

I show that the firing precision is determined largely by the light intensity rather than by temperature. Moreover, a better firing precision barely improves the information rate, which closely follows the mean firing rate. Altogether, my results suggest that the robustness of the motion information processing against temperature variations depends on the quality of the input signal. Furthermore, flies seem to use the input signal-to-noise ratio to improve the information rate and reduce the time-scale of the response simultaneously, by increasing the mean firing rate, rather than the firing precision.

Chapter 2

Introduction

2.1 Motivation

To comprehend the underlying principles of neural computation, it is important to understand how sensory information is represented in the nervous system.

Sensory information processing is a complex task for several reasons. One of them is the limited dynamic range sensory neurons have to encode sensory signals that frequently range over several orders of magnitude. To avoid saturation or loss of sensitivity, sensory neurons have to continually adjust their gains. In vision, for example, light intensity spans over eight orders of magnitude during the day and around three orders in an hour [194], whereas the dynamic range of the membrane potential of the photoreceptor cells covers about two orders of magnitude [110, 8].

Another problem in sensory information processing is noise, which can be inherent to the sensory signal, or intrinsic to the sensory system. Signals that have a discrete character, like odor concentration or light intensity, pose an additional challenge to receptors cells, since their concentrations continuously fluctuate. In the same way, noise sources at cellular or network level arise from thermal-dependent random fluctuations in the concen-

tration of signaling molecules [56]. To which extent internal and external noises contribute to the total noise in the system is still elusive. Some studies put forth that the variability observed in neural signals is due mainly to noise in the sensory signal [9, 17, 115, 132], whereas other studies claim that in certain conditions, the internal noise might be the bottleneck for information processing [65, 53, 112, 111]. In some cases, noise can even improve information transmission [114, 45] or enhance the system dynamics [39, 187], which makes the characterization of the noise impact in the system performance even more challenging.

To counteract undesired noise effects, signals are usually averaged across time and across parallel processing units, yielding a constant trade-off between processing reliability and temporal and spatial resolutions. The representation of sensory information is therefore a dynamic process that can be completely understood only if the adaptation mechanisms the system uses to deal with internal and external perturbations are taken into account.

Since neural signals are eventually represented by sequences of identical action potentials, it is assumed that the information about the signal is contained in the temporal pattern of spikes [186, 151, 27]. The noise in the system is therefore manifested by the spike timing variability, which can be quantified by recording the neural responses to multiple presentations of the same stimulus.

A convenient measure of information content [166] in the response about the stimulus is defined as the number of stimuli that could be distinguished based on the response symbols, that is, spike sequences of certain duration, usually shorter than the behaviorally relevant time-scale of the animal. Thus, the amount of information transmitted by a neuron depends on how many and how precisely spikes can be fired within such an encoding window.

A compensation mechanism against an increase of the noise level could, for instance, maintain the same amount of information by augmenting the encoding window, firing more spikes, or both, limited by functional requirements and energy constraints. An efficient

information representation would contain the most of information using the least of resources, and it has indeed been suggested that sensory systems approach such optimal representation strategies [5, 108, 193, 4, 23, 167, 173].

The aim of this work is to explore the issues discussed above using motion vision in the fly as a model system. Specifically, the following questions will be addressed:

- To what extent does the amount of sensory information in the neural representation vary, when the quality of the input signal and the internal state of the system change?
- How do noise and gain influence the information content, coding efficiency and temporal scale of the representation?

To analyze these issues, responses from the motion sensitive neuron H1 to a time-varying stimulus were recorded. The quality of the input signal was controlled by varying the mean light level and the system state was changed by regulating the temperature.

Although the effect of temperature on the nervous system has been extensively studied since the early days of modern electrophysiology [1, 89, 144, 130, 93], it is still not easy to predict the consequences of temperature changes in the system performance. Even though all biophysical and biochemical processes depend on temperature [43] - e.g. diffusion, chemical equilibrium and reaction kinetics - compensatory mechanisms might easily emerge in such complex systems that have elaborated regulatory pathways and whose components have different thermal dependences [93, 156].

Temperature is an environmental property which is behaviorally relevant for *Calliphora* flies, since they do not actively thermoregulate, like some bees, moths and dragonflies [122, 80]. Flies body temperature closely follows the temperature of the surrounding environment, because their lower mass, high body surface area, and absence of heavy insulation facilitate heat exchange. Thus, in addition to daily thermal variations, which can be more than 10 ° C, flies experience short-term body temperature changes. For example, direct

exposition to sunlight rises their body temperature by about 6 ° C within a minute [202].

Despite changes in the body temperature, *Calliphora* flies are active over a wide temperature range - from $10-12°$ C, where activity ceases [57], up to around 38° C [54], which is the median lethal temperature. In some extreme cases, females were able to fly and lay eggs in carrion at ambient temperatures of about 5 ° C [57].

In summary, flies behave robustly over a temperature range in which the kinetics of biochemical reactions vary between three and fourfold and their visual system adapts to wide variations of signal amplitude and noise. The analysis about how and to which extent the sensory system compensates for such perturbations is not only ecologically relevant, but also might help us to comprehend the underlying principles of robustness in biological systems.

In the next section, a brief overview about the fly's visual system will be presented, with focus on the motion pathway from the photoreceptors to H1. Aspects relevant for information processing as well as comparison between the effects of light and temperature in the system will be highlighted whenever possible. Finally, the main results of a set of studies that motivated this investigation will be discussed in some detail and the aims of this work will be briefly summarized.

2.2 Motion vision overview

2.2.1 Phototransduction

Motion vision starts with the transduction of light into electrical signal in the photoreceptor cells. In flies, eight photoreceptor cells are found in each ommatidium, an optical apparatus composed by a lens, a cone and pigment cells [28, 21, 72]. These structures focus the light into the distal tip of a specialized region of the photoreceptor membrane called rhabdom, which works as waveguide, trapping the light into it [192, 196, 174] (fig.

2.1 A). The rhabdom is formed by a stack of tube-like structures, the microvilli, which have a high concentration of rhodopsin molecules. Each microvillus is thought to be an elementary light transduction unit.

The phototransduction cascade is an inositol phospholipid signaling pathway [126, 74, 128, 172] - when the rhodopsin absorbs the energy of a photon, it changes its configuration, activating a G-protein, which in turn activates a phospolipase C (PLC). The activated PLC hydrolyzes $PI(4,5)P_2$ [1] into IP_3[2] and diacylglycerol (DAG) (fig. 2.1 B). The mechanism that opens the trp[3] and trpl channels is not completely understood, but DAG - or one of its metabolites (PUFAs[4])- and calcium are necessary to open the channels. When the channels open, calcium flows into the cell and triggers several feedback mechanisms that regulate the termination of the response. In addition, calcium changes the gain of the transduction cascade [126, 69, 74, 134]. How exactly calcium acts in the cascade is however unknown. The final product of the cascade is a quantum bump, a depolarization of the membrane for a short period of the time.

The daily dynamic range of light intensities varies up to eight orders of magnitude, whereas the dynamic range of the membrane potential is around 60mv [110, 194]. When light intensity decreases, the photoreceptor sensitivity increases in such a way, that a single photon is able to generate a detectable bump in the photoreceptor membrane [75]. This high sensitivity leads to two negative consequences, however. First, temporal resolution is reduced - the bump duration can reach up to 40 ms at low light levels (at 20° C), whereas at high levels it is around 5ms [153]. Considering that the behaviorally relevant temporal scale for flying flies can be as short as 100 ms, long delays in the first stages of the visual system can reduce the animal's performance. Second, the randomness of photon arrival makes the membrane potential noisy. This photon noise seems to be responsible for about

[1] phosphatidylinositol 4,5 - bisphosphate
[2] inositol 1,4,5 - triphosphate
[3] transient receptor potential
[4] polyunsaturated fatty acids

50% of the total photoreceptor noise at low light intensities [111, 35], but its consequences downstream the visual system are still elusive [65, 17, 115]. When the mean light intensity increases, the bump amplitude, latency and duration are reduced [97, 91].

The time constant of the photoreceptor membrane is regulated by a voltage-dependent potassium conductance [199], which matches the membrane bandwidth to the time scale of the transduction cascade.

Another gain mechanism is the pseudo pupil - calcium induces the migration of pig-

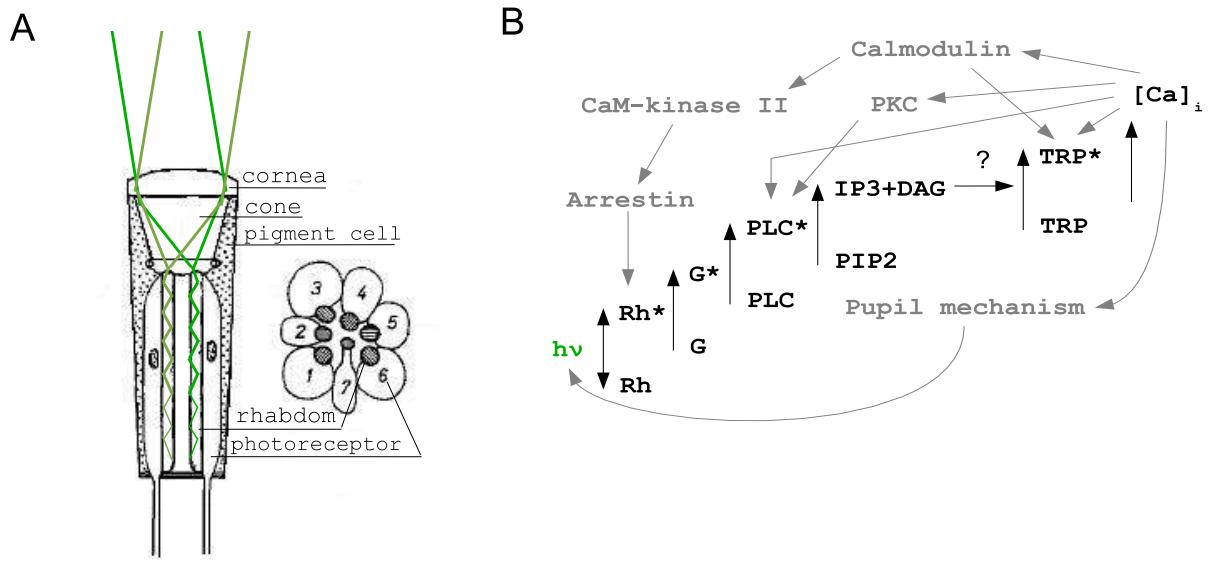

Figure 2.1: Fly's visual system. **A.** Schematic representation of an ommatidium, showing transversal and horizontal sections. Green lines represents the light pathway. **B.** The phototransduction cascade. Rhodopsin absorbs the energy of a photon and initiates a biochemical cascade which culminates with the opening of the trp channels. Gray arrows indicates feedback mechanisms. Details in the text. **A** adapted from ref. [100]

.

ment molecules from the cytoplasm to nearby the rhabdom. These molecules regulate the amount of light that travels within the rhabdom, by altering the refraction index of the boundary between rhabdom and cytoplasm [101, 103]. The pupil mechanism also shifts the spectral sensitivity of the photoreceptors [75, 154, 175], which is set by the rhodopsin molecule - in the peripheral photoreceptors R1-6, the peak of absorption is around 490

nm. There is an additional peak in the UV region, caused by the sensitizing pigment 3-hydroxyretinol, which transfers the energy absorbed in the UV to the 3-hydroxyretinal, the rhodopsin chromophore [102]. The photoreceptors R1-6 are involved in motion detection, since the motion sensitive cells in the lobula plate have spectral sensitivities similar to R1-6 [11, 81]. The central photoreceptors R7-8, involved in color vision, have several types of rhodopsin, depending on the position of the photoreceptors in the eye [75, 72].

An increase in temperature also accelerates the photoreceptor response [61, 200, 153, 185]. The bump duration and latency are reduced almost to one third for a temperature increase of $10°C$. The bump amplitude, however, seems to be robust against temperature changes [153]. In *Drosophila* photoreceptors, the information rate increases by almost sevenfold when temperature rises $10°C$ [96].

In several invertebrates, the pupil mechanism also depends on temperature - pigment migration increases with warming, even in absence of light (see ref. [133] and references therein).

2.2.2 Retina-Lamina signal transmission

The first optic lobe (fig. 2.2 A), the lamina, is formed by an array of anatomical units, called cartridges. Each cartridge comprises at least 16 identified neurons [168, 182]: the large monopolar cells (LMCs) L1-L5, the efferents C2 and C3 and TAN1-TAN3, the basket cell T1 and five amacrine cells. Lateral interactions between cartridges occur via L4, amacrine and possibly glial cells [168, 22].

Each cartridge receives the output of six photoreceptors R1-6, from different ommatidia, which have the same optical axis [99]. Thus, the light of a given spatial position in the environment is gathered by six different lenses, transduced at six different receptor cells, whose signals, then, are pooled in lamina cartridge. This neural superposition mechanism improves the amount of acquired light by sixfold, without increasing the diameter of the

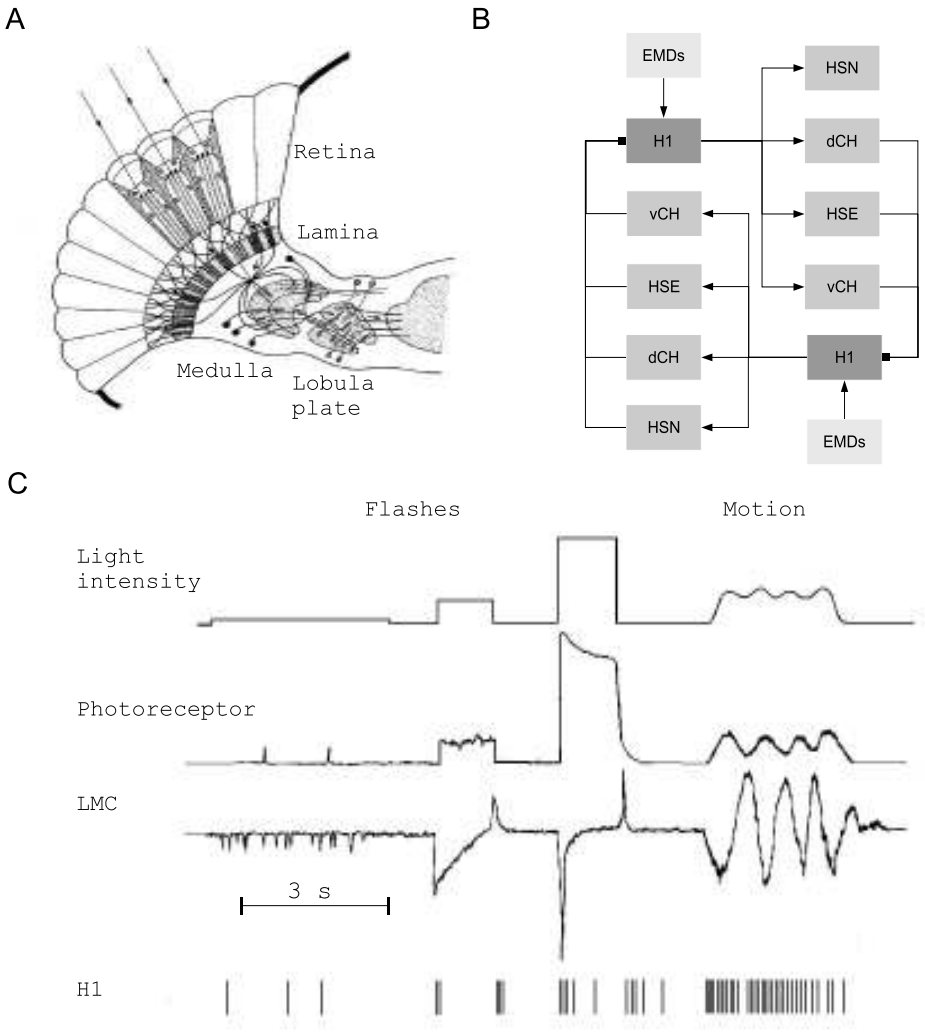

Figure 2.2: Fly's visual system. **A.** Schematic representation of horizontal section of the fly's head, showing the visual neuropils involved in motion processing. **B.** Summary of H1 connections. The H1 in left lobula plate excites the HS and CH cells of the right lobula plate, which in turn inhibit the right H1. Thus, the two H1s mutually inhibit each other via HS and CH cells. HS cells also receive input from elementary motion detectors (not shown) **C.** Schematic representation showing responses of a photoreceptor in retina, of a large monopolar cell in the lamina and the H1 in the lobula plate to light flashes and motion of a periodic square wave grating image. **A** adapted from ref. [100] and **C** from ref. [116]

.

lenses, and therefore keeping the spatial resolution constant. The axons of photoreceptors R7-8 bypass the cartridges of the lamina and terminate in the next neuropil, the medulla.

The cells responsible for pooling the photoreceptors signals are the large monopolar cells L1-L3 and amacrine cells. The L2 and amacrine cells also feedback onto photoreceptors [168]. During synaptic transmission between photoreceptors and LMC's, the signal is inverted - photoreceptors release histamine [73], which in turn opens chloride channels in the LMC membrane. Moreover, the synaptic transmission works as a high pass filter - sustained signals are suppressed and transient signals emphasized (fig. 2.2 C). Thus, transient increases in the light intensity hyperpolarize the LMCs, whereas sudden reductions depolarize them. The transmission gain changes with light intensity, so that the operation point of the photoreceptor-LMC synapses is kept at the region where the characteristic curve has maximal slope [111, 189]. LMC responses match the statistics of contrasts found in natural environments, maximizing thus the information transmission of naturalistic stimuli [108].

In the lamina cartridge, photoreceptors' axons are connected by gap junctions [149]. The purpose of these connections is not yet completely understood. It was suggested that they could reduce the noise before the chemical synapses between photoreceptors and LMCs [149] or even lower the coupling between photoreptors, due to the extracellular potential in the cartridge [191]. Interesting, high frequency oscillations (≈200Hz) can be observed in the LMC responses when the photoreceptors are not stimulated in balance [190], a condition that certainly occurs at low light intensities (see also fig. 2.2 C). About half of the noise measured at LMCs is added during synaptic transmission [111].

2.2.3 Motion detection in the medulla

For motion detection, it is necessary to take at least two spatial points of the visual field into account. Several response properties of motion sensitive cells, in particular their dependence on pattern features other than velocity [14, 52], are explained by the Reichardt correlation model for elementary motion detection [147]. In the simplest version of the model, one of the inputs is delayed and multiplied by the second input. The physiological

implementation of the model in the fly's visual system is elusive. The first neuropil in which motion sensitive cells are found is the medulla [44, 64, 40, 125]. Like the lamina, the medulla is also organized in a retinotopic fashion, as an array of columns. Two pathways for motion processing from the retina to the tangential cells in lobula plate, which integrate the output of the elementary motion detectors, were proposed - the first involves the photoreceptors R1-6, the large monopolar cell L2, the transmedullary cell Tm1 and the lobular bushy T5 cell; the second pathway is constituted by the R1-6 photoreceptors, the L1, the intrinsic transmedullary iTm and bushy T4 cells, localized in the medulla [44, 181, 180]. Whether the T4 or T5 cells provide input to the H1 is unknown.

2.2.4 Integration of motion information in the lobula plate

The lobula plate is composed by at least 21 classes of neurons [124, 182, 78]. Among them, there are two well studied classes of directional selective wide field neurons - the vertical and horizontal cells [47, 77, 49, 18], which provide motion information to the neck [183, 66, 85] and flight motor systems [58, 10, 12, 62, 79, 66].

The H1 is part of the horizontal system - it is excited by horizontal ipsilateral regressive motion (from back towards front), and inhibited by ipsilateral progressive motion. The H1 projects its axon (diameter of $\approx 5\mu$m and length of $\approx 1200\mu$m) to the contralateral lobula plate and provides excitatory input for two horizontal cells (HS) and two centrifugal cells (CH). These cells, in turn, inhibit the ipsilateral H1 [78] (fig. 2.2 B).

The H1's dendritic arborization covers the whole lobula plate, and consequently, its receptive field covers almost the whole ipsilateral visual field, since the mapping is retinotopic [78]. The maximal sensitivity is found in the centro-equatorial region (elevation 0°, azimuth -15°) [48, 78, 105]. In addition to the position of the stimulus in the visual field, H1 is also sensitive to several other parameters of the visual stimulus. For example, its firing rate increases with image contrast [13, 148, 197] and size [78, 113, 13]. For the image

size, the range covered by the system is remarkable - from a single elementary motion detector, when just two photoreceptor cells are stimulated [150, 163], up to the stimulation of the entire visual field, when about 5000 ommatidia (in *Calliphora*) are stimulated simultaneously.

Equally remarkable is the sensitivity of the system to light intensity [48, 124] - H1 responses to single photons can be detected [117], and motion responses for intensities above 2.5 10^{-4} cd m^{-2} have been observed [163]. Finally, H1 responses adapt to the statistics of image velocity [120, 23, 55, 16, 158] and to light intensity flicker [37, 15]. When flicker stimulus is applied prior to a velocity pulse, the firing rate decays faster to the spontaneous firing level.

2.2.5 H1's outdoor experiments

Recent studies measured H1 responses in the field, at naturalistic conditions. Flies were mounted in rotating supports, whose angular velocity could be controlled. One of the studies measured H1 responses to sinusoidal velocity, at several conditions of light intensity and temperature. The authors found that on average, the mean firing rate increased 85% for a 10 °C difference and barely changed with light intensity [53]. The authors also reported that the spontaneous firing rate did not vary consistently with temperature, a result that was supported by another study of the same group, done at controlled laboratory conditions [198]. This later study also analyzed H1 responses for velocity steps of 4Hz temporal frequency and reported that the steady-state mean firing rate increased by about 60%, when the temperature rose from 18-20 to 26-28 °C. The latency was reduced by about 10ms in the same temperature interval [198]. The authors also claimed that the H1 reliability increased with temperature, by calculating the signal to noise ratio of the spike count within a window of 100ms. However, such an analysis does not reveal whether the firing precision changes, and that is for two reasons. First, since the mean firing rate

increases as well, it is not possible to separate the contributions of the firing precision from the increased rate combined with H1 refractoriness. Second, the velocity is constant for the steady-state responses. Therefore, there is no temporal event that can trigger H1 spikes precisely. Although the authors reported the SNR of the transient responses as well, they used the same coarse time-scale of 100 ms. Moreover, the authors observed that the slope of the firing rate after stimulus onset did not change with temperature, which is an indication that firing precision was conserved.

A second study measured H1 responses outdoor to a time-varying angular velocity similar to free-flight trajectories [115]. This study observed an increase of the information content of the response when the light intensity rose and suggested that it was due to the firing precision, which also improved with light. However, as pointed out in reference [53], the authors did not report the temperature of the experiments, nor did they consider the effect of firing rate, which also increased with light intensity, and could be responsible for the improved information rate [204, 17, 161, 83]. Indeed, the authors observed that the noise entropy did not change with light intensity [115], which indicates that the improved firing precision weakly contributed to the information rate. In addition, the information rates were estimated using a fixed encoding window of 30 ms for all acquisitions, independent of light intensity. If the system trades noise by time-scale, as commented before, the information content between different conditions would not take such adaptation mechanism into account, possibly underestimating the information estimation at conditions of better input signal-to-noise ratios.

2.3 Goals

The studies summarized above left several questions open, which will be addressed in this work. First, although they showed that the firing precision increases with light intensity, the temperature contribution to it could not be clearly defined. Second, it was also not possible to evaluate how the firing precision influences the information content, since the firing rate and precision varied together. Third, the trade-off between noise and response time-scale was not considered. Finally, the effects of temperature and light intensity on some response properties of photoreceptors are interdependent [185, 153], and thus, effects on H1 responses might also be interdependent. Unfortunately, the only study that took both temperature and light intensity simultaneously into account over a wide range of conditions measured just the H1 mean firing rate [53].

To address these problems, I recorded H1 responses to a time-dependent stimulus at 42

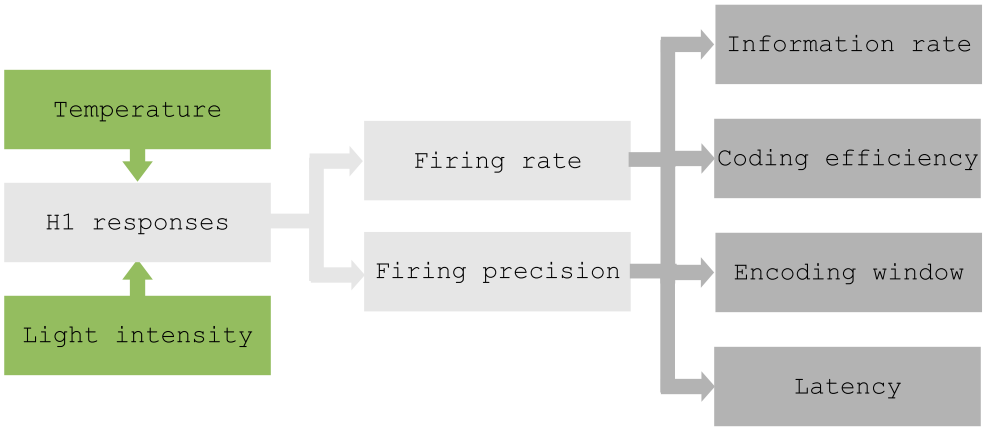

Figure 2.3: The goals of this work are to map out the effects of temperature and light intensity on H1 responses and to determine the contribution of the firing rate and precision to the amount of motion information transmitted and time-scale of the system.

different conditions of light intensity and temperature. The aims are to investigate how H1 responses vary with these environmental perturbations and to determine the contribution of the firing precision and rate to information rates, coding efficiencies and optimal time-scales for information transmission.

Chapter 3

Materials and Methods

3.1 Preparation

Calliphora vicina flies were maintained in the department stock at 19-22° C, 50-60% relative humidity and 12h-12h light-dark cycle. Flies between seven and fourteen days old (after eclosion) were used in the experiments. Flies were anesthetized with CO_2 and the dorsal part of their thoraxes were waxed to a small piece of glass. Their heads were bent toward the ventral part of their thoraxes and waxed to them. Wings, legs and antenna were immobilized with wax. Care was taken to avoid unnecessary heating during waxing. A small cut was done in the back of their heads to get access to the brains. The air sacs that cover the lobula plate were pushed to the side, but the tracheae were left as intact as possible. Flies were then transfered to a metallic case which enclosed their entire bodies, except their heads.

3.2 Temperature control

The temperature of metallic case was controlled by a Peltier device attached to it. To isolate the head thermally from the environment, a soft airstream at temperature approximately of the temperature of metallic case was blown frontally on the head (fig. 3.1 A).

The stability of the head temperature was tested in three flies. Temperature was

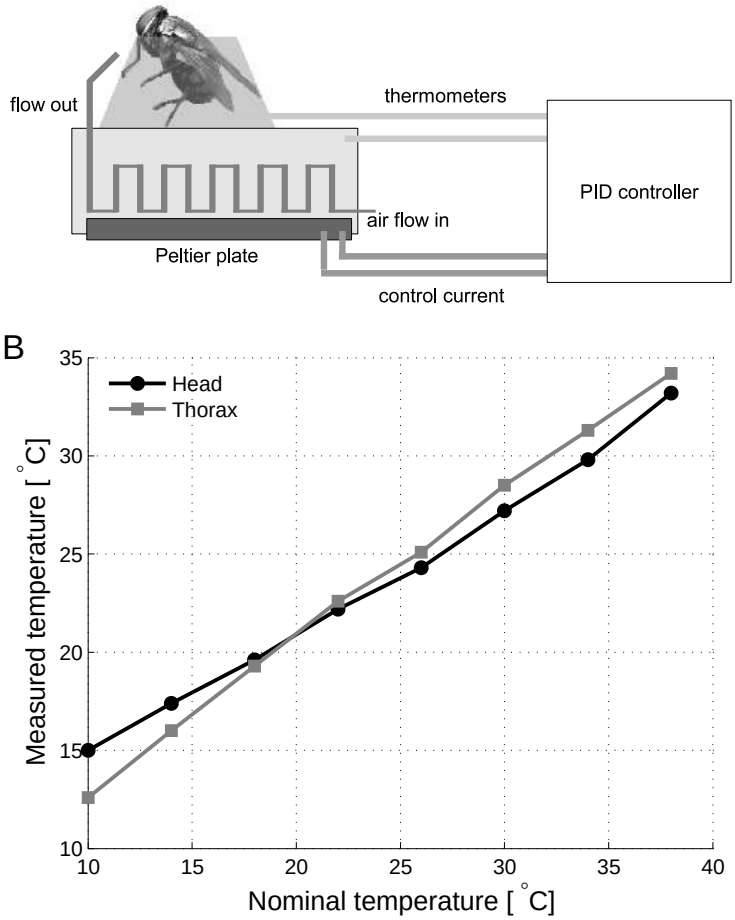

Figure 3.1: Temperature control. **A.** Schematic representation of the setup to control the fly temperature. The airflow used to thermally isolate the head from the environment entered into the heat exchanger at ambient temperature and left it at the temperature of the exchanger. The temperature of the Ringer's solution, which was periodically added to head through a glass electrode (not shown), is controlled in similar way. **B.** Body temperature as a function of the nominal temperature of the heat exchanger.

measured using a microthermoprobe (AD instruments) and an thermometer (GMH3210,

Greisinger electronics, Germany). It was not possible to record head temperature and H1 responses simultaneously. Thus, a relation between the nominal temperature of the exchanger and the measured temperature in the head for three flies was used to infer the head temperature of all acquisitions (fig. 3.1 B). Peltier device, PID controller and heat exchanger were built at the MPI workshop.

3.3 Data acquisition and visual stimulation

Tungsten electrodes with impedance of $\approx$ 1MΩ (World Precision Instruments, USA) were used for extracellular recordings from the H1 neuron, which was identified unambiguously by its localization (fig. 3.2) and characteristic response to visual stimuli - excitation to horizontal front-to-back motion and inhibition in the opposite direction. Glass electrodes were used as ground and to load Ringer's solution into the brain to keep it moist. In some experiments, retinograms were also measured. For these experiments, the electrode was impaled into the eye, and the reference electrode was positioned into the head, immediately below the eye.

After amplification (gain of 1.5 10^4) and bandpass filtering (300-3KHz), H1 responses were processed on-line by a threshold unit which generates a pulse of 1.2 ms when the voltage crossed the threshold level, which was adjusted manually. The signal was then sampled at 1 KHz by the analog input of the Visage system (Cambridge Research Systems, UK) and saved in the microcomputer for off-line analysis.

To measure the retinograms and the dependence of the H1's field potentials with temperature at higher sampling rates, a 16 bits AD board (Measurement Computing, USA) was used, because the Visage sample rate is limited to 1KHz. The signal after the filter stage was then sampled at 48KHz, saved in the computer and analyzed off-line. The program that control the acquisitions was written in MATLAB (Mathworks,USA). Pre-

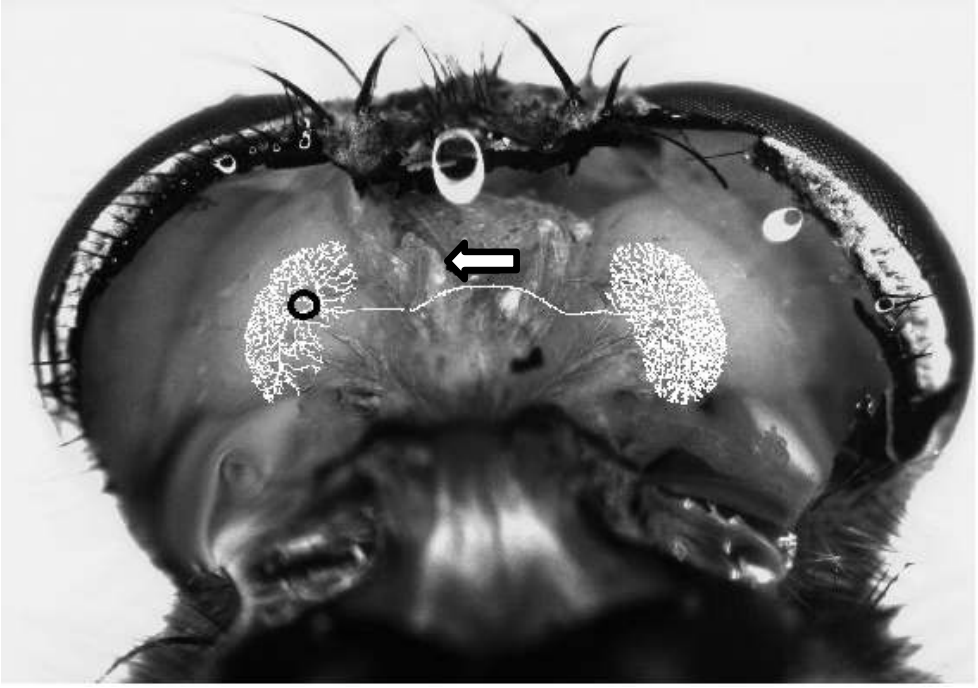

Figure 3.2: Schematic representation of H1 anatomy and position in fly head, shown here fully opened from behind. The arrow indicates the flux of information, and the circle the approximated position of the electrode during recordings. Photo taken by Y. Choe and H1 anatomy adapted from reference [77].

amplifier, amplifier and filters were built at the MPI workshop.

The visual stimulus was presented on CRT-monitor (M21LMAX, Image systems corp., USA) updated at 240 Hz. Flies were positioned twenty centimeters from the front of the monitor, so that just one eye was stimulated, yielding a visual field of 72°x83°, starting at head midline (azimuth=0°). The image used was a square-wave grating with 10° spatial wavelength and contrast of 67%.

The horizontal image velocity v was drawn from a Gauss-Markov process [152, 7], with mean $\mu \approx 0\ ^\circ s^{-1}$, standard deviation $\sigma \approx 40^\circ s^{-1}$ and correlation time of $\varsigma \approx 400$ms. Although the yaw velocity in free flight can reach up to 2000 $^\circ s^{-1}$ during head saccades, most of the velocities between saccades is lower than 100 $^\circ s^{-1}$ [160]. The image velocity

was recursively generated using [7]

$$v(n) = \rho(n)v(n-1) + \Omega(n)\sigma\sqrt{1-\rho^2(n)}$$

where n is time, $\rho(n) = exp(-(n+1)/\varsigma)$ and $\Omega(n)$ is a random number drawn from a Gaussian distribution, using the MATLAB random number generator. For each acquisition, the stimulus, whose duration was ten seconds, was repeated 150 times, with two seconds interval between trials. The image was presented without motion for two minutes before the start of the acquisition, to adapt the photoreceptors to the mean luminance level. The first fifteen trials and the first second of each trial were discarded to avoid accommodation effects and transient responses.

In experiments in which the light intensity was also time-varying, the waveform was also drawn from a Gaussian-Markov process. In these experiments, the visual field was divided horizontally into two separated rectangular regions, in which motion and flicker stimulus could be presented independently. Each region had an extension of 57°x32° and were separated by 10 °. The image pattern inside the rectangles was the same as described above.

In the retinogram experiments, only the light intensity was time-dependent, and the entire visual field of stimulation (72°x83°) was used. The intensity pattern was adapted from the naturalistic light intensity database of van Hateren [194].

The control of stimulus presentation was done using the real-time sequencer of the Visage system, interfaced by a custom software written in MATLAB.

3.4 Data analysis

3.4.1 Pre-analysis

The aim of this work was to measure system performance - variability, reliability and time scale - to encode time-dependent motion information at different conditions of temperature and luminance. To quantify these response properties, it is necessary to record H1's responses to multiple presentations of the same stimulus (fig. 3.3).

An accurate estimation of H1 variability requires that H1's firing properties are stable throughout the acquisition. The response stationarity over trials was then quantified by an accommodation index, defined as the ratio of spike count of the first and hundredth trials (fig. 3.4). Since a higher accommodation rate would overestimate the response variability, only acquisitions with accommodation indexes between 0.7 and 1.3 (338 from 359 acquisitions) were used for further analysis.

The estimation of H1 variability might also be compromised if the responses entrain with refresh rate of the video monitor. The degree of entrainment was measured by the residual power of the mean time-dependent firing rate at 238-242Hz. The mean firing rate was calculated as

$$\lambda(n) =< r(n) >_{trials} \tag{3.1}$$

where <> denotes average and r(n) is an approximation of the instantaneous firing rate for a given trial, defined as the inverse of the interspike intervals, that is,

$$r(n) = \sum_{k=2}^{K} \frac{1}{n_k - n_{k-1}} [U(n_{k-1}) - U(n_k)] \tag{3.2}$$

where $U(n_k) = 1$ for $n \geq n_k$ and 0 otherwise and $n_1, ..., n_K$ were the action potential occurrence times. Power spectra were calculated using the Welch-Bartlett method [121].

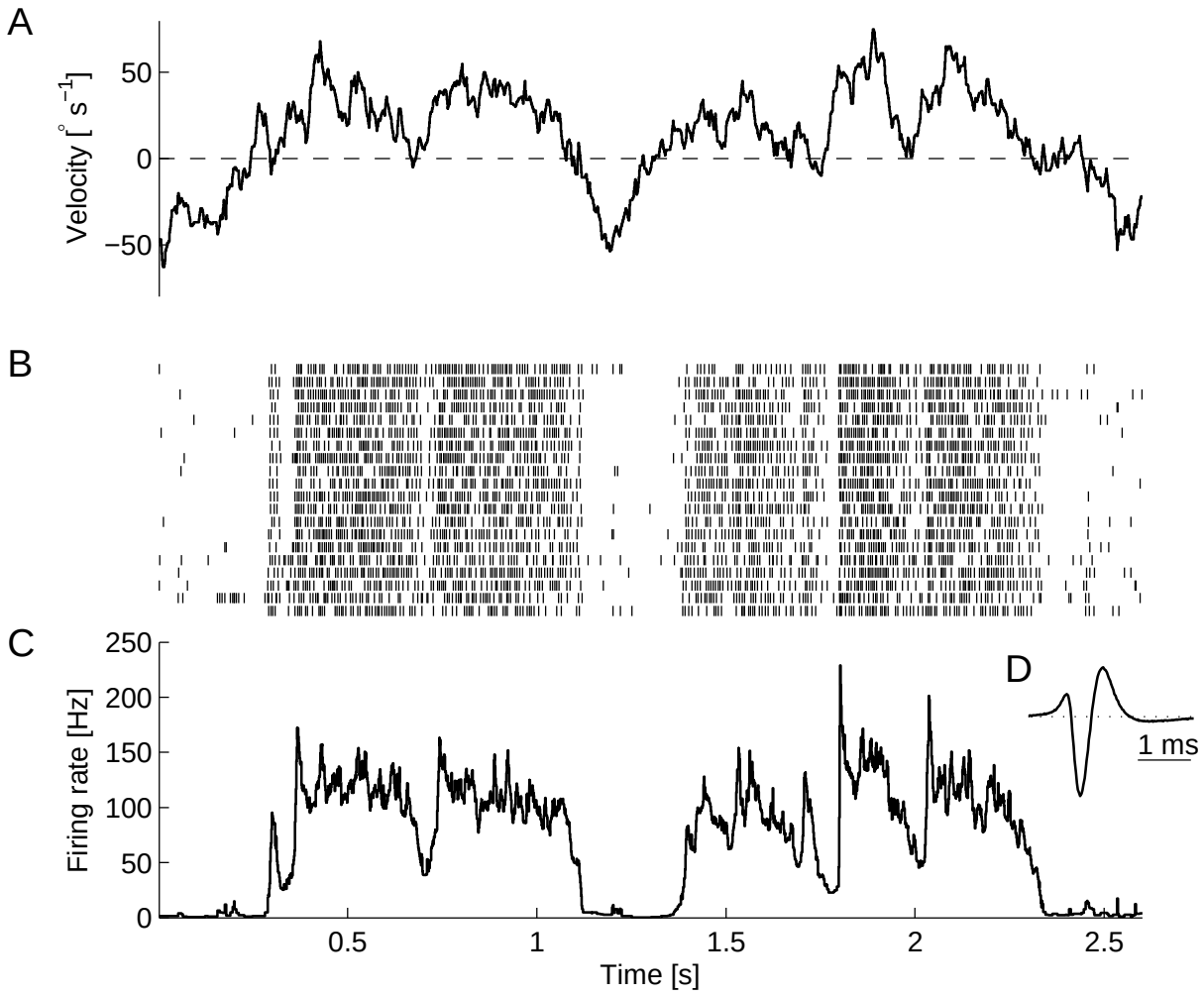

Figure 3.3: H1 responses to the time-varying velocity stimulus. **A.** Two and half seconds of the horizontal velocity of the square-wave grating image as a function of time. **B.**H1 responses to stimulus shown in **A.** Markers represent action potential occurrences. **C.** Averaged instantaneous firing rate. **D.** Average shape of the extracellular field potential. The peak-to-peak amplitude is around 200μ Volts. The signal was band-pass filtered (300-3KHz).

The mean firing rate was first windowed to reduce frequency leakage,

$$\lambda_i(n) = \lambda(iD + n)w(n)$$

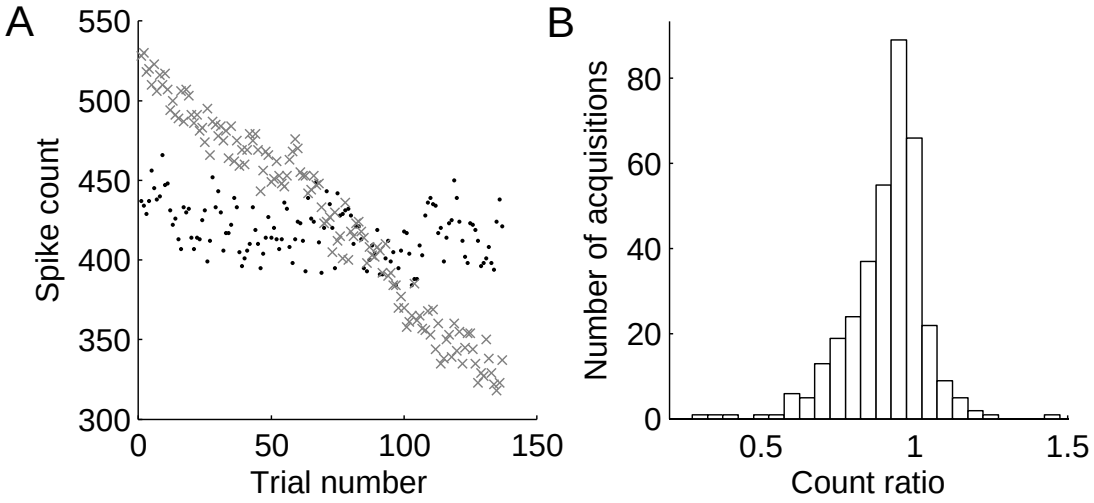

Figure 3.4: Spike count stationarity. **A.**Spike count as a function of the trial number. Examples of mean spike counts for two different flies (crosses and points) with similar mean spike count, but different accommodation rates. **B.** Histogram of the accommodation index of 359 acquisitions.

where

$$w(n) = 1 - (\frac{n - 0.5L}{0.5L})^2$$

is the Welch window, L is the window length and D is the overlap between subsequent windows. The Fourier transform of each windowed segment was calculated as

$$\lambda_i(m) = \sum_{n=0}^{L-1} \lambda_i(n) exp(-\frac{2\pi jmn}{L})$$

and the power spectrum estimated as the averaged power over all windows

$$\Lambda(m) = \frac{1}{L} < |\lambda_i(m)|^2 >_i$$

The sampling frequency used was 1KHz, the window length 512 ms, with overlap of 256ms. The residual power was obtained by removing the linear trends in the spectrum (fig. 3.5). Acquisitions in which the averaged residual power p_Λ within the interval 238-242 Hz was

higher than 0.37 dB (three standard deviations of the p_Λ distribution) were discarded (13 of 359 acquisitions).

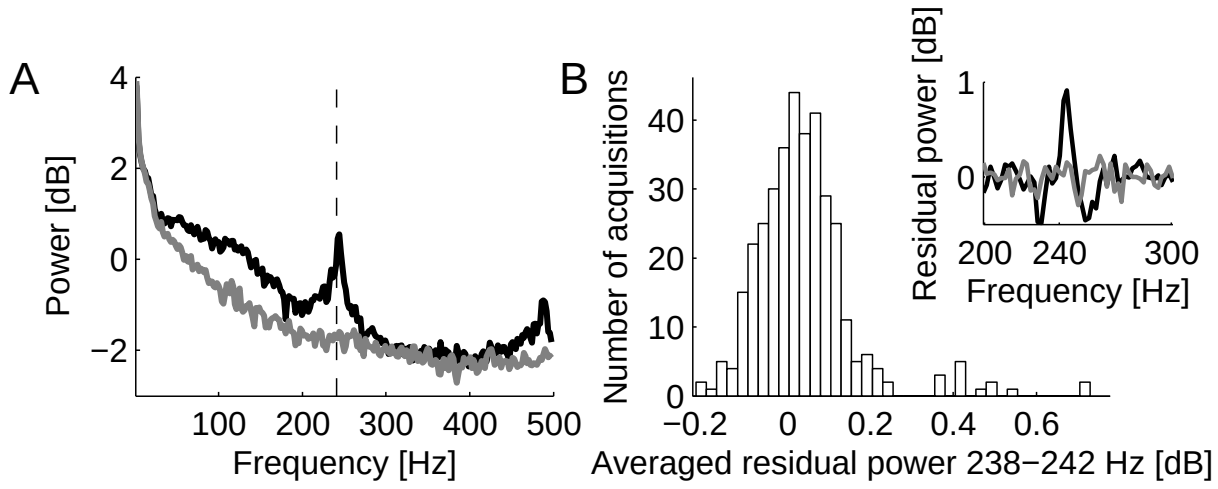

Figure 3.5: Response entrainment to the video refresh rate. **A.** Examples of power-spectra of the average time-varying firing rates of two different flies (black and gray) with similar mean spike count, but different entrainment levels. The refresh rate of the monitor is indicated by the vertical dashed line. **B.** Histogram for all acquisitions of the average residual power near the video refresh frequency. The respective residual power spectra are shown in the inset.

3.4.2 Information theory

The statistical dependence between stimulus and response can be measured by their mutual information [166, 32, 19] defined as

$$I(S;R) = \sum_{\mathbf{s}\in S} \sum_{\mathbf{r}\in R} p(\mathbf{s},\mathbf{r})\ log_2\ \frac{p(\mathbf{s},\mathbf{r})}{p(\mathbf{s})p(\mathbf{r})} \tag{3.3}$$

where S and R are the sets of stimuli and responses and $p(.)$ denotes probability distribution. Stimulus and response were discretized in bins of Δt ms and written as sequences of

words

$$S(L_s, \Delta t, \tau) \equiv \{\mathbf{s_{1},_\tau}, \ldots, \mathbf{s_{K},_\tau}\}$$

$$R(L_r, \Delta t) \equiv \{\mathbf{r_1}, \ldots, \mathbf{r_K}\}$$

where L_s and L_r represent the respective word lengths and τ is the delay of the stimulus to its respective response. To estimate of the probability distribution $p(s, r)$ in equation 3.3, three stimulus parameters should be chosen - the stimulus length L_s, the delay τ and the amplitude resolution of s, Δs. In addition, although the velocity v is the only time-dependent part of the stimulus in the majority of the experiments, it is not known a priori whether H1 encodes just stimulus velocity, or some function of it. To avoid these problems [36, 184], $p(r, s)$ can be substituted by $p(s|r)p(r)$ in equation 3.3, yielding

$$I(S;R) = -\sum_{r\in R, s\in S} p(r,s)\ log_2\ p(s) + \sum_{r\in R, s\in S} p(r,s)\ log_2\ p(s|r) = H(S) - H(S|R)$$

where $H(S)$ is the entropy of the stimuli and $H(S|R)$ is the conditional entropy of the stimuli given the responses. The mutual information is symmetric, thus $H(S) - H(S|R) = H(R) - H(R|S)$. Because the same stimulus was presented multiple times, $H(R|S)$ can be calculated as $H(R|n)$, where n is time, discretized. The information rate for a given window length L_r and bin width Δt can then be estimated as

$$\widehat{I}(S;R) = \frac{1}{L_r}[H(R) - H(R|n)] \tag{3.4}$$

without the explicit determination of stimulus parameters. The entropies $H(R)$ and $H(R|n)$ were corrected for sampling bias using the methods explained in detail in the next section. A bin width Δt of 2 ms and window length L_r from 2 to 20 ms were used to calculate $\widehat{I}(R;S)$. A bin width of 2ms is the coarsest width in which the responses are still binary.

The influence of spike-timing precision in the information rate was inferred by comparing the information rates calculated using two different bin widths: in the *timing encoding* mode, the bin width Δt is fixed to 2ms; in the *count encoding* mode, the bin width Δt is equal to L_r. Thus, in the *timing encoding* mode, the exact positions of the spikes within the encoding window were taken into account to calculate the information rate, whereas in the *count encoding* mode just the number of spikes within the window was considered. The difference between the information rates of the two modes reveals how much information is carried by the precise spike times.

The optimal encoding window L_r^* was defined as

$$L_r^* = \arg \max_{L_r} \widehat{I}(R;S)$$

For a better approximation of L_r^*, the search of the maximum was done in a spline interpolated approximation of $\widehat{I}(R;S)$ (fig. 3.6).

The response latency was defined as the τ that maximizes equation 3.3 [98], making the assumption that H1 encodes velocity and setting $L_s = 1$, $\Delta v = 1^\circ s^{-1}$ and $L_r = L_r^*$, that is

$$\tau^* = \arg \max_{\tau} \frac{I(V;R)}{L_r^*}$$

Standard gradient ascent with an amortization step was used to find points near the maximum of $I(V;R)$, which were then then interpolated using cubic spline. The τ^* was found by direct search in the interpolated points.

The influence of the length of integration window L_s on the determination of τ^* was tested for two different dimension-reduced representations of v - the averaged velocity within L_s and the first two principal components. Despite changes on $I(V;R)/L_r^*$, no significant difference on τ^* was detected for L_s between 2 and maximal L_s allowed by causality - $n_v + L_s + \tau < n_r$, where n_v and n_r are respective starting times of the words **v**

and **r**.

The coding efficiency was defined as

$$\eta = \frac{H(R) - H(R|n)}{H(R)} \tag{3.5}$$

and calculated for *timing* and *count* modes.

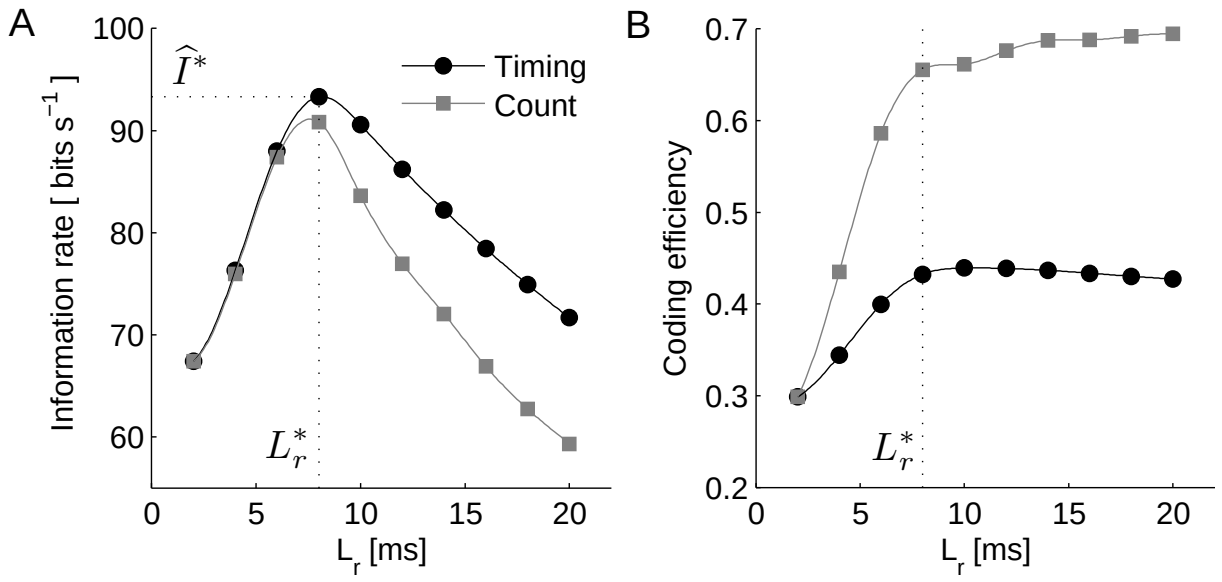

Figure 3.6: Optimal information rate. **A.** Example of the information rate as a function of the encoding window, for timing and count encoding modes. L_r^* is the encoding window at which the information rate is maximized. **B.** Respective coding efficiencies.

3.4.3 Bias correction

The bias of the entropy estimator $H = H(R)$, obtained using a set of N observations $\{\mathbf{k_1}, \ldots, \mathbf{k_N}\}$, is the difference between its expected value and the true entropy **H**. A wide variety of methods to correct for bias is available in the literature (for recent reviews, see references [87, 195, 138]). Here I used the jackknife [145, 51] combined with surrogate

datasets to reduce bias. Assuming that the bias can be expanded in power series of $1/N$

$$< H > -\mathbf{H} = \frac{b_1}{N} + \frac{b_2}{N^2} + \dots \tag{3.6}$$

where the coefficients b_i do not depend on N, the jackknife estimator of $\mathbf{H}$ is

$$\widetilde{H} = NH - (N-1)H_{(.)} \tag{3.7}$$

where

$$H_{(.)} = \frac{1}{N}\sum_{i=k_1}^{k_N} H_i \tag{3.8}$$

and $H_i = H(\mathbf{k_1}, \dots, \mathbf{k_{i-1}}, \mathbf{k_{i+1}}, \dots, \mathbf{k_N})$ is the estimation of the entropy H without using the response $\mathbf{k_i}$. Asymptotically, $\widetilde{H}$ is biased[1] only to order $1/N^2$ [145, 162]. However, for small datasets $\widetilde{H}$ might not eliminate the bias completely. A pilot acquisition with 596 trials was use to estimated the residual bias after jackknife correction as a function of the dataset size. The residual bias was estimated as the difference between the information rate calculated using the corresponding number of trials and the 'true' information rate - calculated using all trials.

Two additional corrections to eliminate the residual bias were proposed. The first one used data shuffling [131, 135]. The residual bias was considerably reduced by subtracting the square-root of the information rate of a surrogate dataset, in which the interspike intervals within each trial were shuffled (fig.3.7). The corrected rate was then calculated

[1] it can be easily seem [162] by calculating the expectation of $\widetilde{H}$

$$< \widetilde{H} >= N < H > -(N-1) < H_{(.)} >$$

$$< \widetilde{H} >= N(\mathbf{H} + \frac{b_1}{N} + \frac{b_2}{N^2} + \dots) - (N-1)(\mathbf{H} + \frac{b_1}{N-1} + \frac{b_2}{(N-1)^2} + \dots)$$

$$< \widetilde{H} > -\mathbf{H} = \frac{-b_2}{N(N-1)} + o(\frac{1}{N^3})$$

as

$$\widehat{I}(R;S) = I_{jack} - \sqrt{I_{shuffle}} \tag{3.9}$$

The surrogated information $I_{shuffle}$ was also jackknifed. The squared-root was determined empirically, by observing the difference of the growth rate of the jackknifed and shuffled information rates when L_r increased.

Using this method, a minimum of one hundred trials was necessary to reduce the residual bias to around 1% of the true information rate, for a Δt of 2ms. For 150 trials, the maximal error was less than 0.3%.

In the second method, artificial data were created from the original acquisition, using

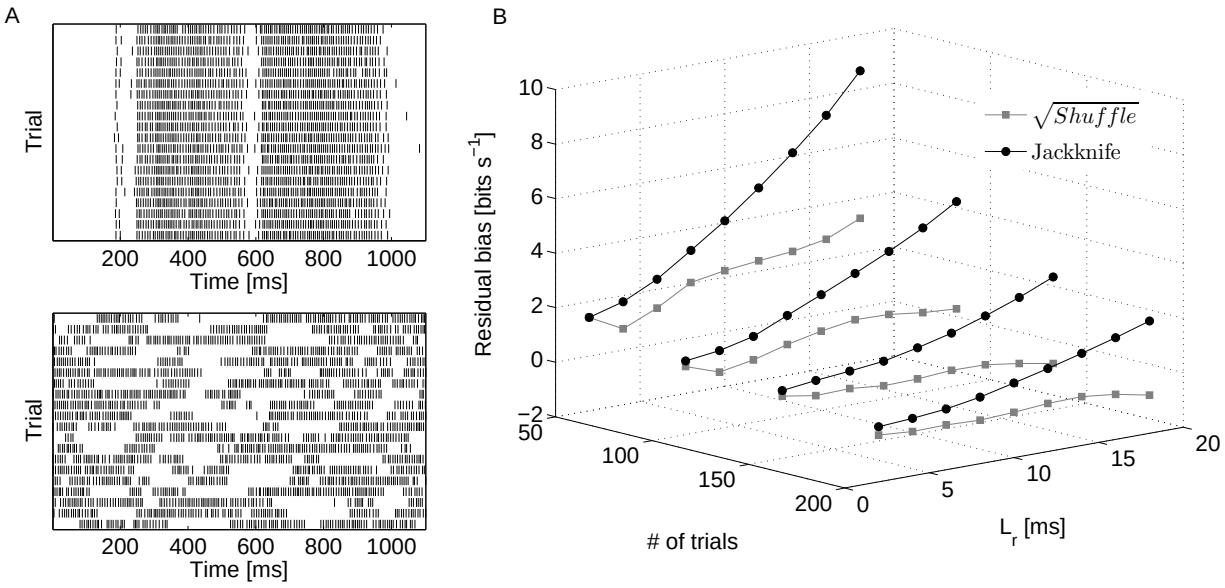

Figure 3.7: Bias reduction. **A.** Original acquisition and its surrogate, with shuffled interspike intervals. **B.** Residual bias for a bin width Δt of 2 ms, as a function of the number of trials and encoding window length, after jackknife and jackknife-shuffle surrogate correction.

estimations of the firing rate (eq. 3.2) and local interspike interval distributions (ISI). Responses were generated by the rejection method [142]: for a given time n, an action

potential was generated if $r(n) < c$, where c is a (uniform) random number between 0 and c_{max}. The firing rate $r(n)$ was then multiplied by a local recovery function, defined as the cumulative probability distribution of the ISI at time n. The procedure is then repeated for subsequent times till the end of the trial.

The mean firing rate of the generated data depended on c_{max}. The values of c_{max} that matched the range of the spike count of the original data were found using several datasets of 50 trials, created using different c_{max} values within a wide range. The spike counts of those datasets were calculated, and spline interpolated to find the best c_{max} values.

From the chosen c_{max} values, approximately 3000 trials were generated. One thousand of them were selected by rejection sampling, to match the count distribution of the original acquisition. The residual bias was then calculated as the difference between the information rates using 135 and 1000 trials of the artificial dataset, and subtracted from the information rate calculated from the original acquisition.

The methods described above, $\sqrt{Suffle}$ and *Monte-Carlo*, had superior performance compared with other non-parametric methods tested (fig. 3.8).

3.4.4 Classification theory

The discrimination between the probability distributions of a determined response property, e.g. ISI distributions, was quantified using the Chernoff distance, defined as [32, 94]

$$D_c(p_a, p_b) = -\min_{0\leq\lambda\leq 1} \; log \sum_x p_a^{\lambda}(x)\; p_b^{1-\lambda}(x) \tag{3.10}$$

For a optimal likelihood ratio classifier, the Chernoff distance bounds the total error probability [32]

$$\frac{\log\ P_e}{N} \leq D_c(p_a, p_b)$$

where N is dataset size.

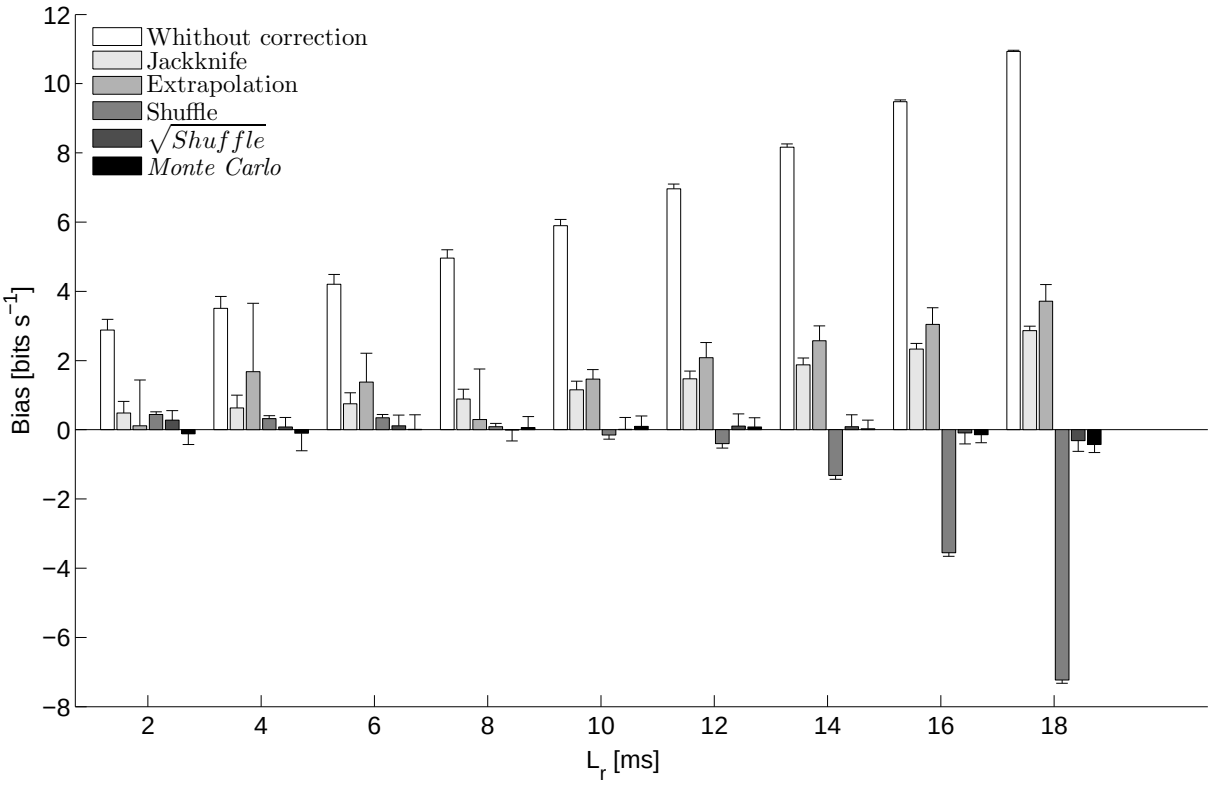

Figure 3.8: Comparison of several non-parametric bias correction methods. Error bars are standard deviations for five estimations using datasets of 150 trials randomly chosen from the 596 trials of a pilot acquisition.

3.4.5 Statistical analysis

Statistical significance was assessed by non-parametric statistical tests - Wilcoxon sign rank for single, Wilcoxon rank sum for double and Kruskal-Wallis for multiple comparisons. The sample size for each condition for double comparison was estimated as 8 independent measurements (two-sided test, detected difference of 10%, with size of 0.08 and power of 0.85) [63]. If not stated otherwise, error bars reported in the graphs are confidence intervals ($\alpha = 0.08$), calculated using non-parametric bootstrap with one thousand replications [205]. To measure the correlation between random variables, either mutual information or Spearman rank correlation coefficient was used.

3.4.6 Temperature and luminance coefficients

The temperature coefficient Q_{10} of a determined response property f was defined as

$$Q_{10}(f) = \frac{f(25^\circ\ C)}{f(15^\circ\ C)}$$

where $f(25^\circ\ C)$ and $f(15^\circ\ C)$ were obtained from a linear least-square fit of the data. The coefficient of luminance K_{1000} was defined as

$$K_{1000}(f) = \frac{f(100\ cd\ m^{-2})}{f(0.01\ cd\ m^{-2})}$$

and calculated in the same way as Q_{10}.

Chapter 4

Results

The first part of this chapter shows the effect of temperature and light intensity on basic H1 response properties, without motion stimulation. The goal was to verify to which extent the system state is influenced by these disturbances.

In sequence, the response properties to motion stimulation will be analyzed. It will be shown that temperature and light intensity act interdependently in some response characteristics, like in the mean firing rate. Other response properties, like the spike jitter, are influenced mostly by one of perturbations.

Finally, the information rate, coding efficiency and time-scales of the responses will be shown and the contributions of firing rate and spike jitter to the information rate will be investigated. In addition, a comparison between count and timing encoding modes will be made, at scales where information rate is maximized.

4.1 Extracellular field potentials

The shape of the action potential influences the time scale and gain of synaptic transmission, because the influx of calcium in the presynaptic terminal is driven by the calcium electrochemical driving-force, which is set by the interaction between the kinetics of the calcium channels and the shape of the action potential [157, 20].

Action potential duration and amplitude depend on the time courses of sodium and potassium conductances, which vary with temperature [93, 86]. Because warming speeds the gating rate of ion channels, the duration reduces when temperature rises [127, 143, 76, 2, 93, 130, 67, 144, 82, 118]. The amplitude, however, depends on how the time-courses of the conductances vary - it can be reduced [127, 2, 178, 93] or increased [93, 67, 130] with warming, depending on the preparation.

The measured H1's field potential arises from a sum of currents of neighbor regions of the axon

$$\Phi_e = \frac{1}{4\pi\sigma_e}\int_L \frac{i_m\, dx}{\sqrt{(x-x_p)^2+(y-y_p)^2+(z-z_p)^2}}$$

where L is the total length of the region of the axon, (x_p, y_p, z_p) is the position of the electrode, σ_e is the extracellular conductivity and i_m is the transmembrane current [139, 179, 90]. Assuming that the axon has just sodium and potassium conductances, the triphasic shape of the H1 field potential (fig 4.1) can be interpreted as formed by three currents: a capacitive, with time constant τ_c; an inward sodium, with peak width of δw and an outward potassium, with time constant τ_k.

No consistence changes in the peak amplitudes were observed ($p > 0.5$ for all peaks, n=4). The duration was reduced when temperature rose (fig. 4.1 C). The Q_{10} of time-scales of the three different phases were similar (≈ 0.82) - note that when the time-axis was scaled by the width of the sodium peak (fig 4.1 B), the shape of the potentials overlapped.

The duration of the observed extracellular potential depends on the propagation veloc-

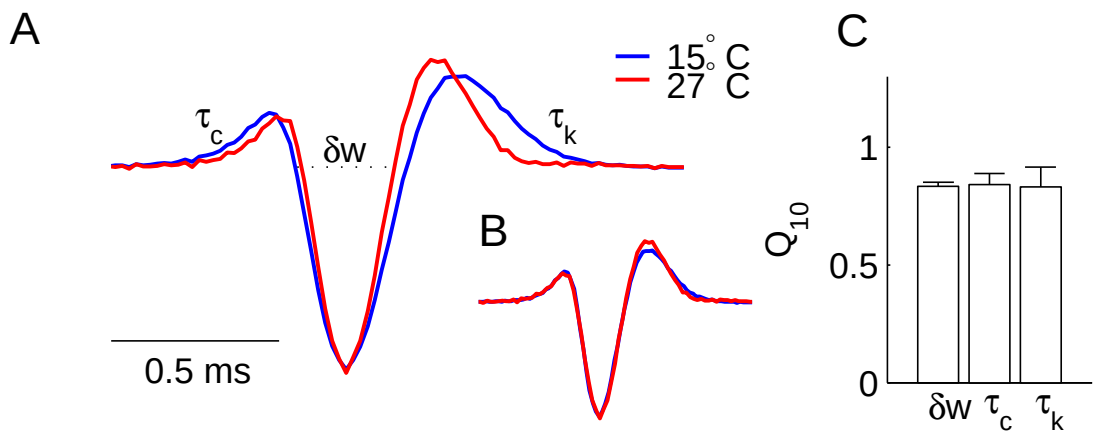

Figure 4.1: Dependence of the extracellular action potential waveform on temperature. **A.** Average extracellular field potentials of the same cell at two different temperatures. Signals were bandpass filtered (300-3KHz). **B.** The same waveforms shown in **A** , with time axis scaled by the width of the sodium peak, δw. **C.** Averaged Q_{10} of the time constants and peak width, for four different flies. Errors bars are bootstrap confidence levels.

ity of the action potential and on its spatial extension. It is not possible to separate their contributions based solely on the observation of the potential. However, if it is assumed that the major contribution was due to changes in the propagation velocity, the Q_{10} for conduction velocity would be approximately 1.2.

4.2 Spontaneous firing rate

Since H1 pools the output of several thousands of elementary motion detectors, it is expected that spontaneous events that occur along the pathway upstream H1 will modify its spontaneous activity. Such synaptic bombardment can change neuron's gain [31], increase its response variability by reducing input synchronization [187, 56, 165], or even enhance the detection of subthreshold input signals [39, 88, 114, 45].

Spontaneous vesicle release [140, 170, 76, 6, 93] and spontaneous neural discharge [26, 60, 92, 82, 93, 130, 144] usually increase with warming. However, previous studies

found that H1's spontaneous firing rate barely changes with temperature [198, 53]. Nevertheless, in these investigations the spontaneous rate was measured in presence of static illumination, which probably masked the temperature effect, since H1's spontaneous rate also increases as light intensity increases [117, 48, 124].

To verify whether temperature influences the spontaneous activity in the system, in-

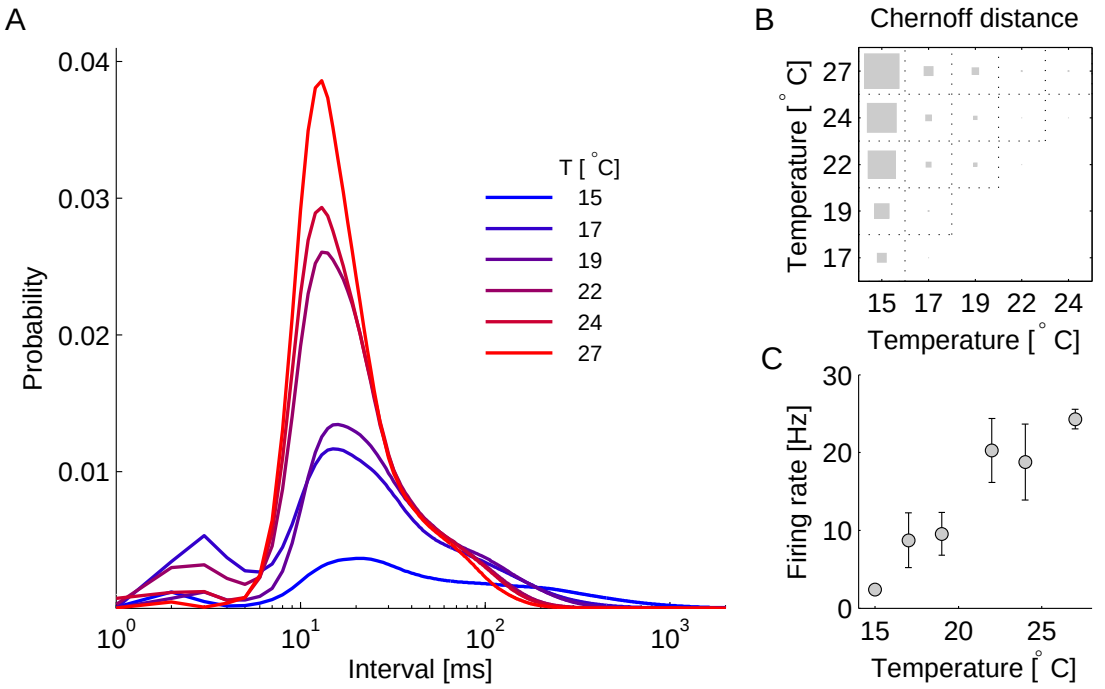

Figure 4.2: Spontaneous activity as a function of temperature. **A.** ISI distributions as a function of temperature, estimated using a Gaussian kernel, with optimized width [46]. Each record lasted 7.5 minutes. Data from three flies were pooled. **B.** Chernoff distances between ISI distributions shown in A. The largest square represent a distance of approximately 0.9, whereas the smallest, 0.03. **C.** Mean firing rate as a function of temperature. Error bars are standard deviations. The Spearman rank correlation coefficient is $\rho = 0.91$ (p=3.1 10^{-5}, n=3 flies).

terspike interval distributions (ISI) were estimated from H1 recordings in the dark (fig. 4.2 A). Short ISIs became more frequent as temperature increased. The average firing rate, calculated as the inverse of the mean interspike interval, had a Q_{10} of 6.42 [3.95;8.38] (mean and confidence interval, $\alpha = 0.08$, n=5 flies). Short interspike intervals (10-100ms)

happened even at lower temperatures, indicating facilitation.

The similarity between distributions was measured using the Chernoff distance, as described in section 3.4.4. Apparently, the distributions were divided into two groups (fig. 4.2 B) - below and above 20 $^{\circ}C$, the temperature which flies were reared.

To test whether light intensity masks the temperature influence in the spontaneous rate, Chernoff distances between ISI distributions at 15 and 27$^{\circ}C$, in the dark and in the presence of static illumination (84 cdm^{-2}) were compared. With visual stimulus, the distance was reduced by approximately fourfold. The Q_{10} of the mean rate reduced from 6.89 in the dark, to 3.34 in the presence of the image.

In summary, the spontaneous activity in the system rose when light intensity or temperature increased. The effects were interdependent, which means that coefficient of temperature depend on the light level. Interdependent effects were also observed in several response properties of flies' photoreceptors [200, 153, 185], like bandwidth, which has a Q_{10} of 3 when cells are dark adapted, and 1.9 when light adapted [185].

4.3 Stimulus-induced firing rate

The amplitude of the time-dependent firing rate (fig. 4.3) was reduced when light intensity or temperature decreased, with exception at 24 $^{\circ}C$, where the amplitudes hardly changed over the entire range of light intensities. For temperatures below 22 $^{\circ}C$, sudden amplitudes changes occurred at 1 cd m^{-2}. Note that for a given temperature, amplitudes were rather constant for light intensities above 9.2 cd m^{-2}.

These trends are easily observed when the mean amplitude of the time-varying rate and the coefficients of temperature and light intensity were calculated (fig. 4.4 A). The coefficient of temperature of the mean rate decreases with light intensity. At lower light

intensities, the mean Q_{10} was above 2, whereas at 84 cdm^{-2}, it was 1.24. Recall that the Q_{10} for the inverse mean interspike interval in the dark was around 6.4, consistently with this trend.

The coefficient of luminance K_{1000} also depends on temperature - it was above 2 for temperatures lower than $22°C$, and around 1.8 at $27°C$. At $24°C$, it was not significantly different from 1 (p=0.92).

A second property of the firing rate that can be observed in fig. 4.3 is the temporal

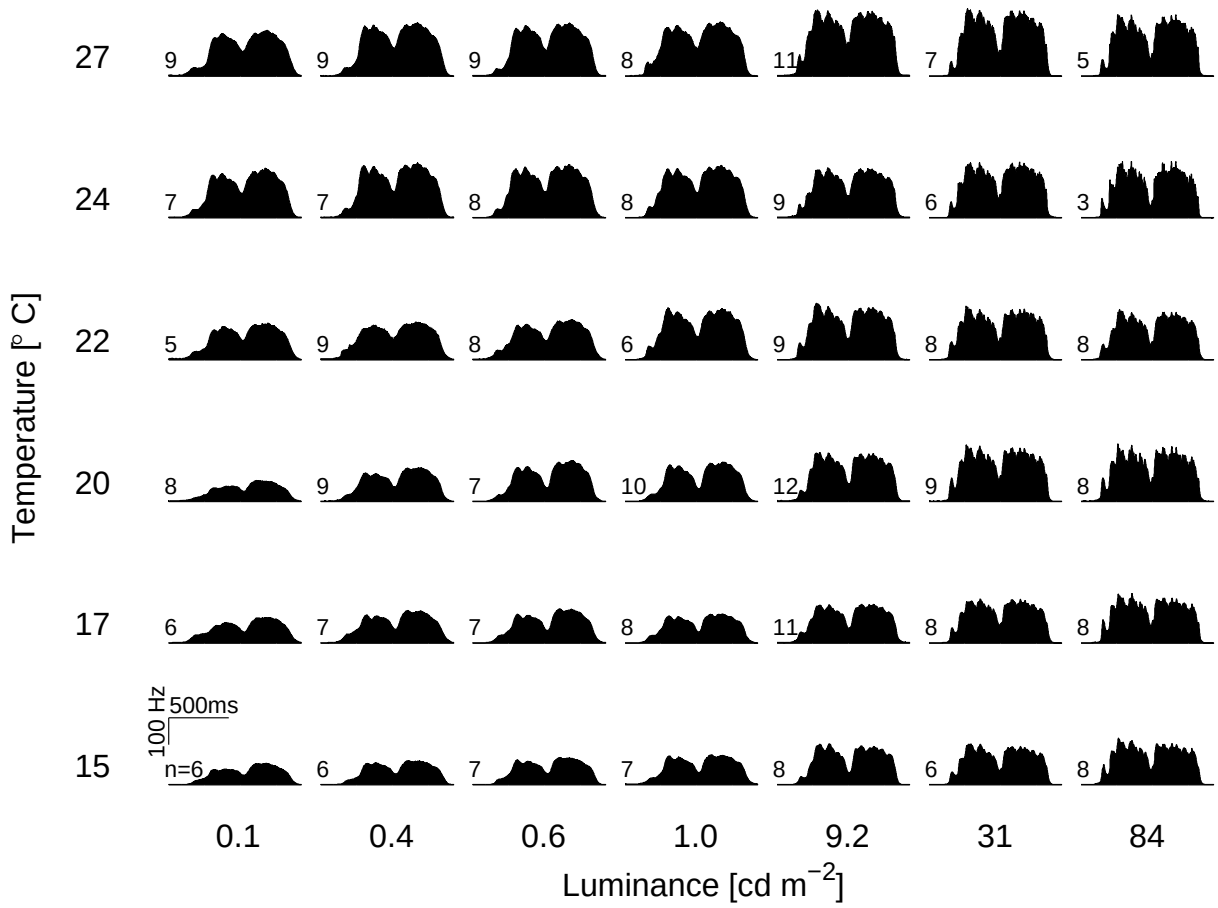

Figure 4.3: Time-varying firing rate. H1's firing rate in response to the first 1.1 seconds of the velocity profile shown in fig. 3.3, as a function of temperature and light intensity. Firing rates were pooled across flies, n is the sample size.

modulation. The modulation indirectly reflects the response variability, since spike jitter

sets the smoothness of the average rate. Somewhat surprisingly, high frequency components were observed in several conditions of temperature and light intensity, despite the fact that mean rates at a given condition were calculated from pooled data of several flies. The temporal modulation of the rate strongly increased with light intensity. The effect of temperature seemed to be more evident at lower light intensities.

To quantify the temporal modulation, the bandwidth of the firing rate was calculated. The bandwidth was defined as the frequency at which the power of the rate was zero decibel. The Q_{10} for modulation varied only slightly with light intensity, and was not significantly different from 1 at 31 (p=0.17) and 84 cd m^{-2} (p=0.53). The K_{1000} for modulation did not show a clear dependence on light intensity - its averaged over temperatures was 4.8.

A more direct, yet local way to quantify the response variability is by measuring the spike timing jitter - the standard deviation of the spike times after some temporal reference (fig. 4.4 C). The reference chosen was a velocity transition, when it becomes positive. Because the firing precision varies with the slope of the velocity, the measurements are not absolute, however.

The effect of temperature on jitter was significant only at 84 cd m^{-2}. When the light intensity increased, the jitter was heavily reduced, with exception at 24°C, where the K_{1000} was not significantly different from 1 (p=0.22).

In summary, the effects of temperature and light intensity on the stimulus-induced firing rate were different. Whereas the mean firing rate had a relatively similar dependence on light intensity and temperature, the temporal modulation and firing dispersion were more strongly influenced by light intensity. Therefore, by varying temperature and light intensity, responses with similar mean rates and different firing dispersions can be obtained. The impact of these response properties in the information rate will be analyzed in a later section.

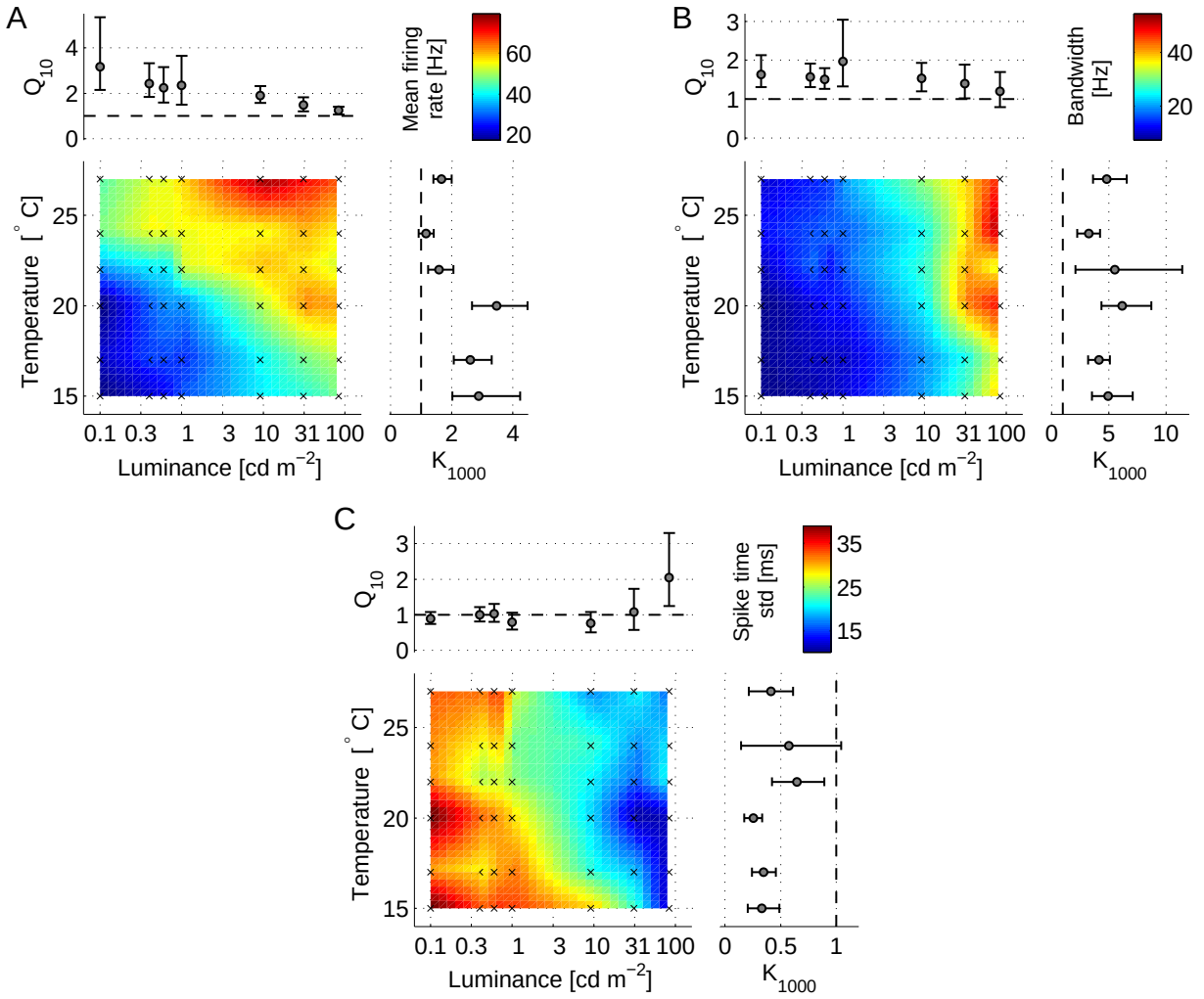

Figure 4.4: Mean firing rate and precision. **A.** Mean firing rate, and **B.** bandwidth and **C.** standard deviation of the time of the first spike fired after a velocity transition (- to +), as a function of light intensity and temperature. Crosses indicate the conditions where the experiments were performed. Color code represents the linear interpolation of the mean values at the experimental points. Q_{10} and K_{1000} are the temperature and luminance coefficients, respectively. Error bars are bootstrap confidence intervals.

4.4 Response stationarity

When the same time-varying stimulus is repeatedly presented to H1, its firing rate usually decays progressively until certain steady state is reached. The accommodation rate of the responses as a function of temperature and light intensity was measured (fig

4.5). The accommodation index (see 3.4.1) was significantly smaller than one at lowers (15-17°C) and higher temperatures (27°C), which means that firing rate was more strongly reduced over trials in these conditions. No clear dependence of the accommodation index on light intensity could be observed. These trends are depicted more directly when the data are pooled across light intensity - the index had a maximum in the middle temperatures and decayed in the boundaries temperatures (p=0.0068, total sample size n=359, 6 groups). At 15°C, the spike count in the 100th trial was on average 85% of the count in the first trial. At temperatures in which the accommodation index was more stable, between 5 and 10 % of the initial count was lost at the 100th trial. For the pooled data across temperature, no significant difference between the light conditions was observed (p=0.28, total sample size n=359, 7 groups).

The accommodation of the response over trials is important for two reasons. First,

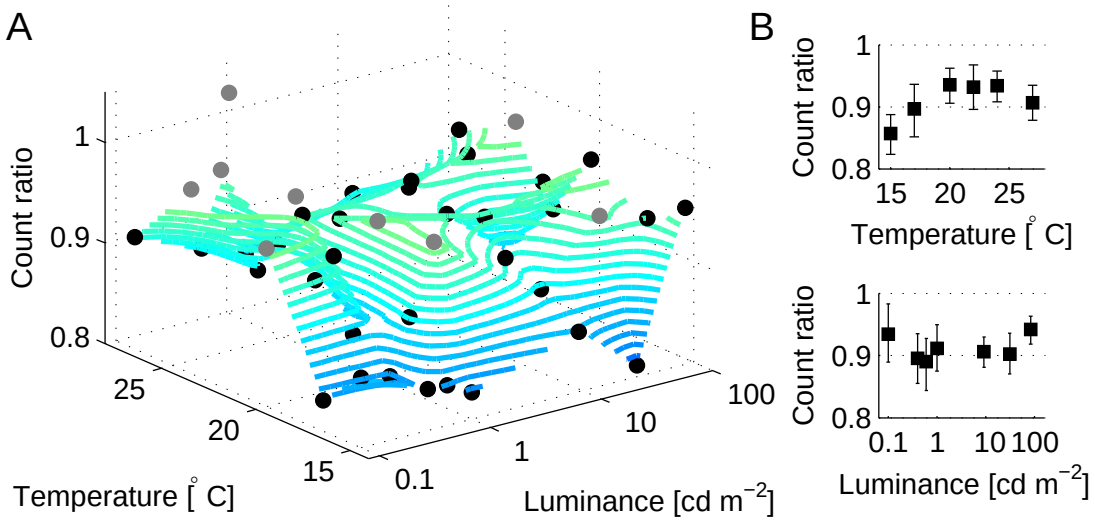

Figure 4.5: Accommodation of spike count as a function of temperature and light intensity. **A** Contour plot of the count ratio, as a function of temperature and light intensity. Dots represent the mean count ratio at the respective condition. Conditions marked with black dots have count ratios significantly different from 1 ($\alpha = 0.08$). **B** Pooled data across light intensity, as a function of temperature. Error bars are bootstrap confidence intervals (n_{min}=55 samples). **C** Pooled data across temperature, as a function of the light intensity (n_{min}=45 samples).

because it is one of the sources of H1's trial-to-trial variability. Second, because it reflects the system reliability to a time-dependent stimulus in a relatively long time-scale (order of several minutes), that occurs even when naturalistic velocities are used to stimulate the fly [83]. This H1's long-term desensitization probably has a contribution from the components upstream the motion pathway. For example, photoreceptors also habituate to multiple presentations of the same stimulus [95]. However, photoreceptors desensitization (at 25 ° C) seems to be higher at low light levels, effect that was not observed in H1 responses.

4.5 Information rate, encoding window and coding efficiency

Information rates were estimated as described in section 3.4.2. The time-scale of the response was considered in the analysis. Thus, instead of extrapolate the entropies values for infinity encoding windows [184], or take a fixed window to compare information rates at different experimental conditions [115], the maximal information rate for each acquisition was taken (fig. 3.6). This analysis was motivated by the fact that behaviorally relevant time scales for flies are around 40ms [107] - encoding windows of infinity length are thus, unrealistic. Moreover, as in the photorecepors, the time-scale to encode information might depend on temperature and light intensity. Thus, a comparison between responses at different conditions using the same fixed window would, at least, fail to take the temporal scale variation into account.

The information rate (*timing* encoding mode) rose when light or temperature increased (fig. 4.6 A). The effects were interdependent - Q_{10} varied with light level and the K_{1000} with temperature. Note the similarity between the information rate and mean firing rate (fig. 4.4 A). Their mean coefficients of temperature and light intensity were not significantly

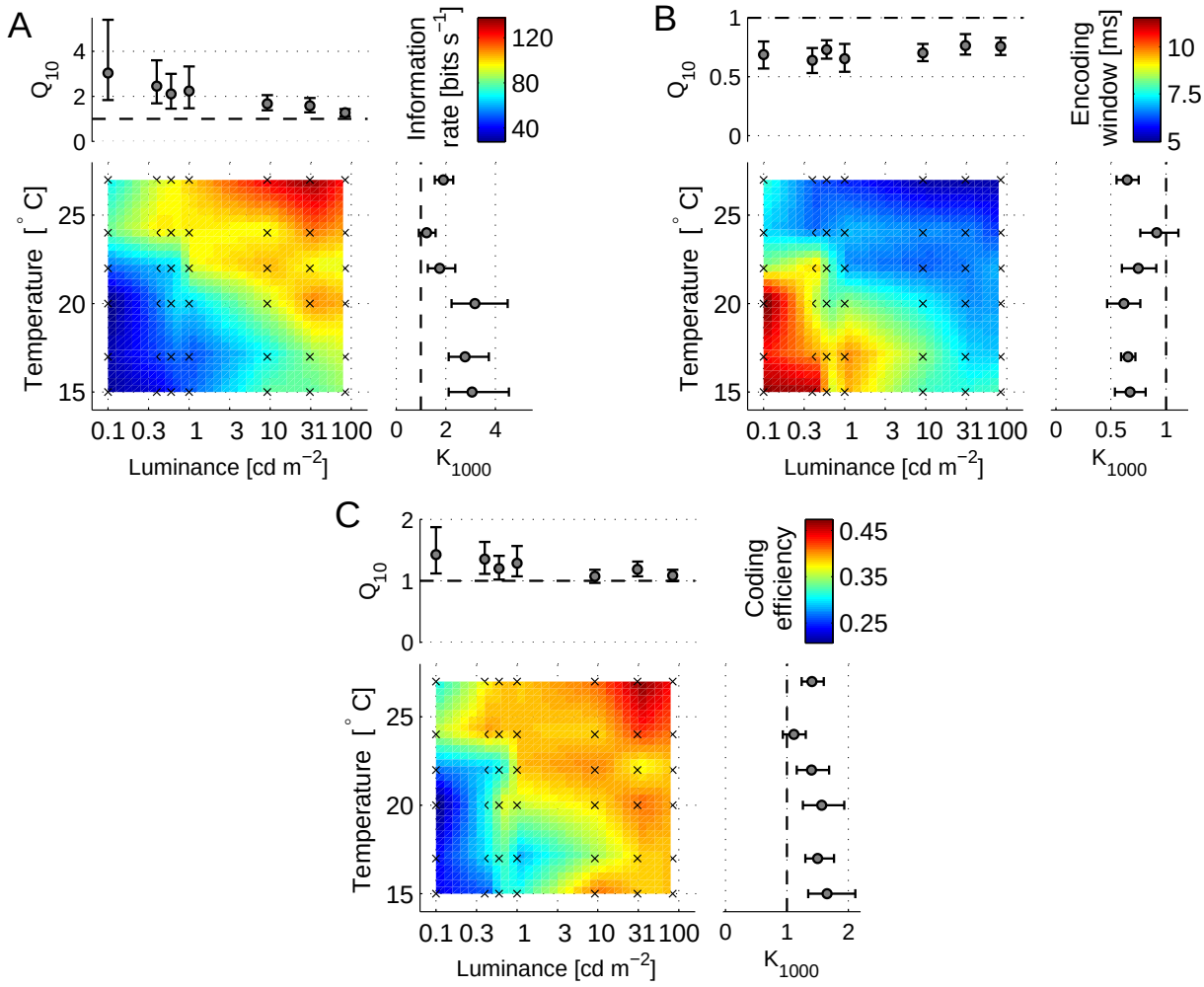

Figure 4.6: **A.** Optimal information rate, **B.** encoding window and **C.** coding efficiency for the timing encoding mode.

different (p>0.2). The mean information rate ranged from around 30 bits s^{-1} at 15° C, 0.1 cd m^{-2}, to 140 bits s^{-1} at 27 ° C, 31 cd m^{-2}.

The optimal encoding window reduced when the light intensity or temperature increased (fig. 4.6 A). The minimum average window was around 5 ms and the maximal, 11 ms. Its Q_{10} did not depend on light level - the mean value was 0.7. However, the K_{1000} depended on temperature. At 24° C, it was not significantly different from 1 (p=0.97). In other temperatures, the mean values were approximately 0.67.

The coding efficiency was around 0.4 for a large set of experimental conditions. Its

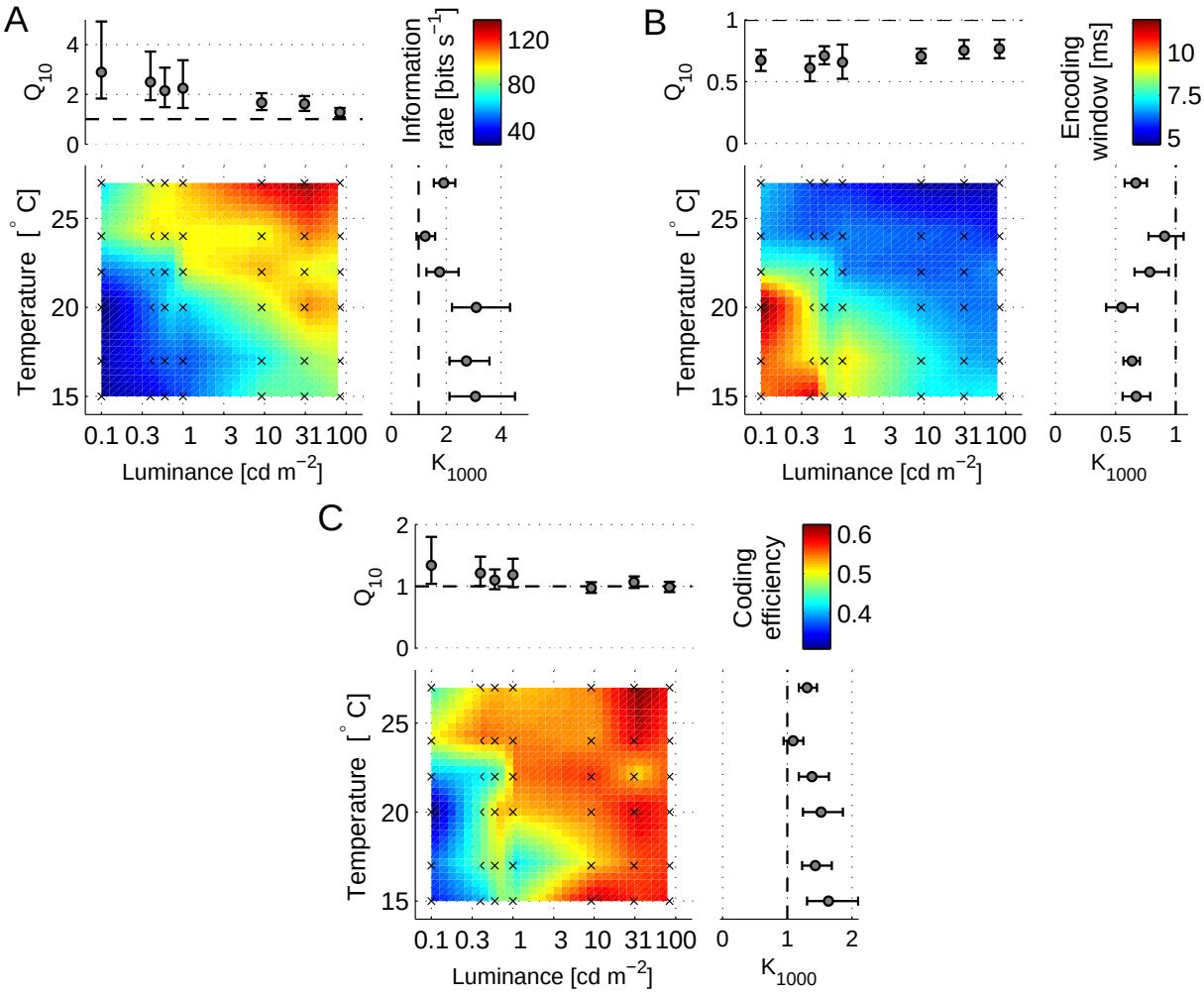

Figure 4.7: **A.** Optimal information rate, **B.** encoding window and **C.** coding efficiency for the count encoding mode.

minimum average value was 0.2 and the maximal 0.47. For light intensities above 1 cd m^{-2}, the $Q_{10}s$ were very close or even not significantly different from 1 (p>0.2).

The K_{1000} for coding efficiency had the same behavior as the K_{1000} for information rate, but was significantly smaller (p=0.03). Observe that the coding efficiency increased more with light level than with temperature - the $K_{1000}s$ were significantly higher than the $Q_{10}s$ (p=0.05).

The results for the count encoding mode, in which the position of the spike within the window is irrelevant, can be seem in figure 4.7.

The information rate in the timing mode was on average 1.06 [0.99;1.14] bits s^{-1} (mean and confidence interval, n=325) higher than in the count mode, at the respective optimal encoding windows. The difference between optimal encoding windows of the two modes was minimal: 0.46 [0.33;0.59] ms.

As in the timing mode, the average coding efficiency in the count mode was relatively

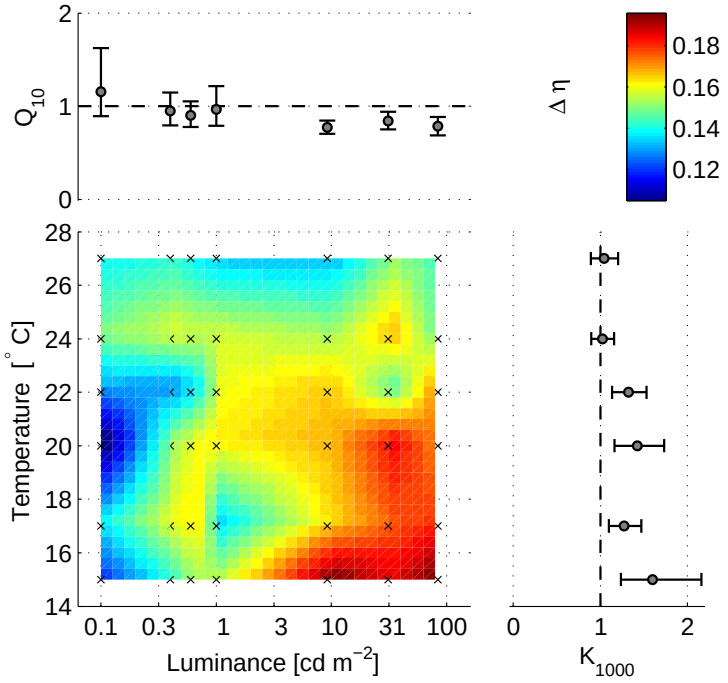

Figure 4.8: The difference between the coding efficiency of the timing and count encoding modes, as a function of temperature and light intensity.

constant over a large set of conditions (fig. 4.7 C). The effect of temperature was significant only at 0.1 cd m^{-2} (p=0.04). The $K_{1000}s$ of the two modes were similar.

The count mode was on average 15% more efficient to encode motion information than the timing mode. The difference between the the coding efficiencies of the two modes was higher at light intensities above 9 cd m^{-2} and temperatures below 20° C (fig. 4.8). The $Q_{10}s$ at these light levels were close to 0.8. Note that the $K_{1000}s$ for temperatures above 22°C were not significantly different from 1. For these temperatures, when the light intensity was reduced, noise and encoding window increased, and the difference between

the coding efficiency of the two modes did not change, which suggests that the augment of the time-scale was a compensation for the increase of the noise level.

When the temperature was reduced, for light intensities above 1 cd m^{-2}, the difference between code efficiencies of the two modes increased, because the firing precision was kept relatively constant whereas the encoding window increased. In this case, there is no trade-off between noise and time-scale.

The relation between H1's firing and information rates has been analyzed before. One

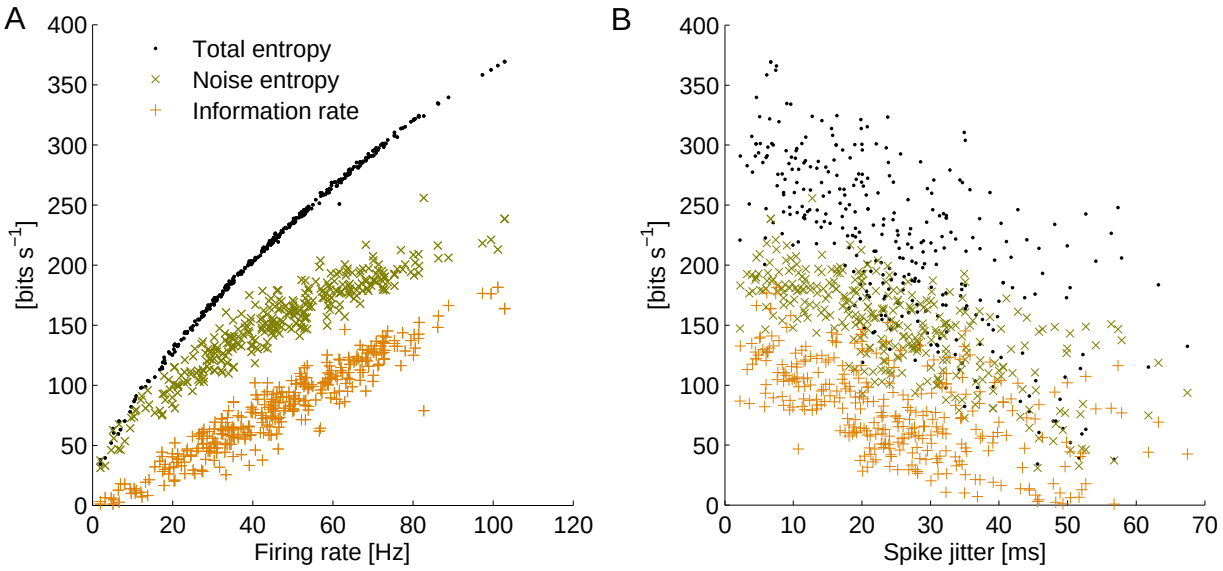

Figure 4.9: Total entropy, noise entropy and information rates as a function of the firing rate **A.** and spike jitter **B.** - the standard deviation of the first spike times after a velocity transition from negative to positive. n=325 recordings.

of the studies analyzed H1 recordings from different flies, whose firing rates were different [161]. A second study manipulated H1's firing rate by changing the image velocity [17] and a third one compare the firing rates before and after H1 accommodation to repeated presentations of the same motion stimulus [83]. In these studies, neither the input signal-to-noise ratio (SNR) nor the internal state of the system was manipulated as in the present work. The results reported above showed that the information rate closely followed the firing rate, even when the input signal-to-noise ratio or the internal state of the system

vary.

It is instructive to analyze the contribution of the total and noise entropies to the information rate (fig. 4.9) as a function of the firing rate and precision. Although total and noise entropies rose as the firing rate increased, the slope of the total entropy was stepper than of the noise entropy, for firing rates above 15 Hz. The correlation coefficients between firing and information rates and between the firing rate and noise entropy were around 0.94, whereas between firing rate and total entropy was 0.99. The major contribution of the firing rate to the information rate was, thus, the increase of the response diversity. The entropies and the information rate were inversely correlated with spike jitter. The correlation coefficients were similar, between -0.6 and -0.7, which indicates again, that the information rate is set by response diversity, rather than noise. However, for other response properties, the effect of the noise might be fundamental, as it will be shown in the next section.

4.6 Latency

The response latency was calculated as described in section 3.4.2. Assuming that the H1 encodes velocity, the latency was defined as the delay in which the mutual information between responses and velocity was maximal.

Previous work defined H1's latency as the time after stimulus onset, at which the mean firing rate reaches some threshold value above the spontaneous activity [197]. Using velocity steps, the authors found a Q_{10} of about 0.7, for images of mean luminance level of 1.4 cd m^{-2}.

The method applied here does not depend on either spontaneous activity or threshold values. Moreover, it considers the possible non-linear relation between velocity and spike trains, and allows the use of complex time-dependent stimuli.

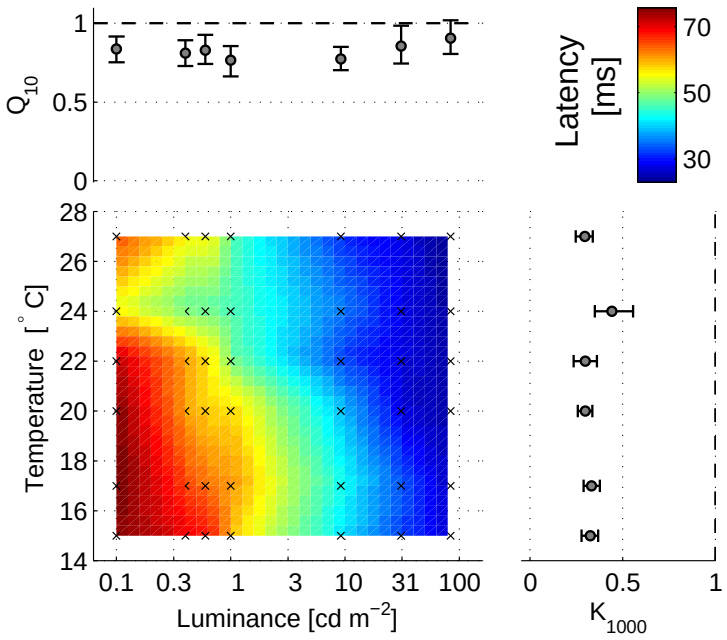

Figure 4.10: Response latency as a function of temperature and light intensity.

The latency as a function of temperature and light intensity is shown in fig. 4.10. The minimum mean value was approximately 22ms, whereas the maximum 75ms. The Q_{10}s were around 0.8 for light intensities below 9.2 cd m^{-2}, and increased slightly for higher light intensities. At 84 cd m^{-2}, it was not significantly different from 1 (p=0.68). Recall that the mean Q_{10} for the encoding window was about 0.7 and for the H1 action potential duration approximately 0.8. To investigate whether the early stages of the visual pathway have similar thermal dependence, retinogram recordings to a time-varying light intensity were made. The image pattern was the same used in H1 experiments. The latency was calculated as the lag that maximizes the mutual information between retinogram and light intensity (fig. 4.11). The Q_{10} for the retinogram latency was approximately 0.75 (n=3 flies). Therefore, temperature variations seems to have effects of similar magnitude on temporal scales of different parts of the system. The Q_{10}s for H1 and retinogram latencies, H1 encoding window and conduction velocity were between 0.7 and 0.8. However, photoreceptors latency to flash stimuli is more thermal-sensitive, with Q_{10} between 0.35 [153]

and 0.66 [185]. The Q_{10} for synaptic delay in clock neurons in the eye of the fly *Musca* is 0.54 [84].

The latency was strongly reduced when the light intensity increased - the mean K_{1000} was 0.33, and almost did not change with temperature. Note that similar values of K_{1000} were obtained for the spike firing precision, but the $K_{1000}s$ for the encoding window were clearly higher.

The reduced temporal resolution of the photoreceptors at low light intensities could

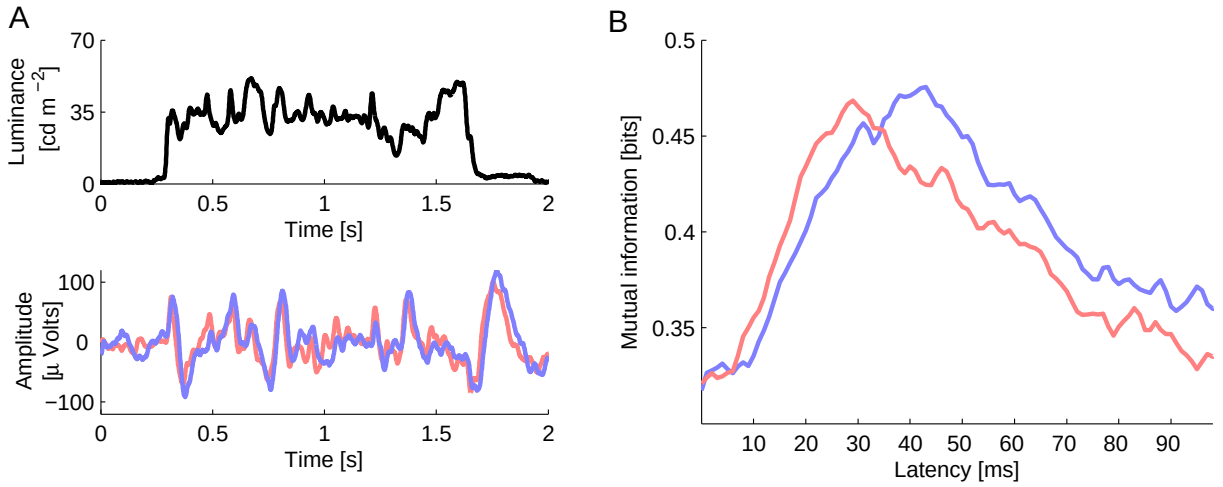

Figure 4.11: Retinograms latency. **A.**Retinograms recordings (lower panel) to light intensity fluctuations (upper panel). Red trace, retinogram measured at 27°C. Blue trace, 17°C. **B.**Latency was calculated as the lag that maximizes the mutual information between light intensity and retinogram.

partially explain the remarkable dependence of the H1's latency with light. A second noise-related contribution to the latency could be the H1's integration process. Desynchronized inputs might lead to a latency increase. At low light levels, the combination of higher gain and the random arrival of photons yields photoreceptor responses with high variability. In addition, the pool of the R1-6 photoreceptors outputs by large monopolar cells in the lamina might generate high frequency oscillations, when the photoreceptors signals are unbalanced (see sec. 2.2.2).

A further experiment was done to investigate whether the contribution of the H1's integration process to the latency was significant. Light intensity modulation was simultaneously presented with motion. The aim of the light modulation was to introduce the high frequency component in the signal, similar to the one that has been observed at photoreceptors and large monopolar cells at low light intensities.

The image was separated into two regions, as described in section 3.3, to determine whether the latency was generated by H1' integration or by processes upstream H1. Within each region, motion and modulation could be presented simultaneously. The time-dependent intensity modulation was Gaussian, with mean of 9.2 cd m^{-2}, standard deviation of 0.9 cd m^{-2} and correlation time of about 24 ms (fig. 4.12 A). Other parameters were tested, in a total of 48 recordings (ten flies), yielding similar results. For the experiment reported below, recordings of five flies at the same experimental conditions were analyzed.

When light intensity was reduced, the response latency was higher after velocity transitions, as can be seem in the time-varying rate shown fig. 4.12 C, recorded from the same fly at three different experimental conditions.

In the experiments with light modulation, the latency increased 10.4 ms ([8.9;12.2], n=5) when motion and light modulation were presented in the same region, in comparison with the presentation of motion alone. The ratio between the latency without and with intensity modulation was about 0.7. Note that the latency seems to be longer after velocity transitions, as in the low light intensity conditions (fig. 4.12 D). The presentation of motion and modulation in different regions did not alter the latency (p=0.95).

The firing precision also decreased with the intensity modulation (ratio of 0.48). For most of the flies, however, the firing precision and reliability after small velocity peaks (v<5 $^{\circ}s^{-1}$) increased when the intensity was modulated, resembling a stochastic resonance effect [106, 39, 88, 114, 45].

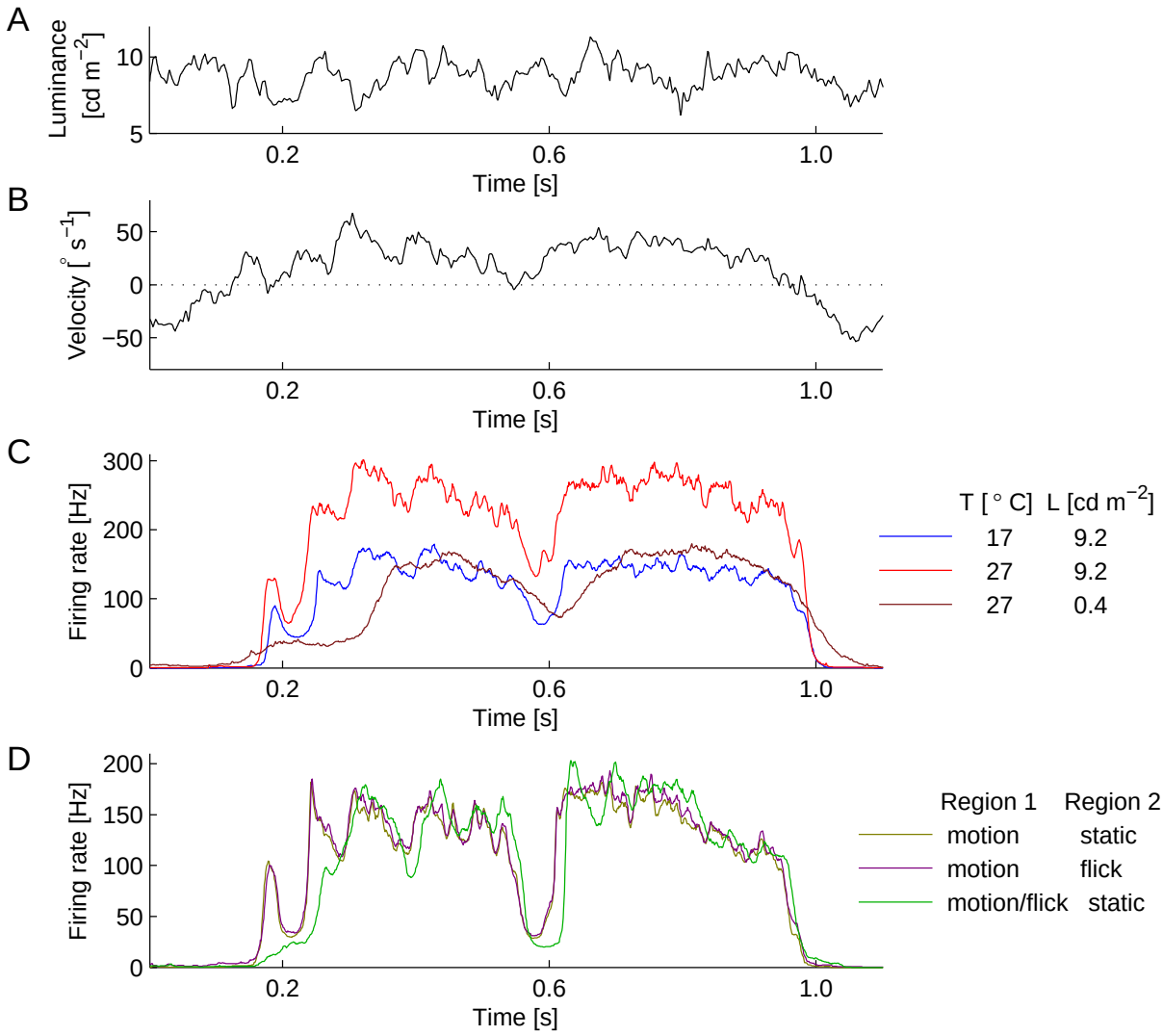

Figure 4.12: **A.** Light intensity modulation as a function of time. **B.** Image velocity. **C.** Time-varying firing rate of the same fly at three different experimental conditions, in response to the velocity shown in **B** . The entire stimulation field was used. **D.** Time-varying firing rate in response to motion and intensity modulation, presented according to the legend. The stimulation field was divided into two separated regions, in which motion and light intensity flicker could be presented simultaneously.

4.7 Summary of the results

In a nutshell, the response properties can be classified into three groups, based on the effect of temperature and light intensity upon them. This can be seem in figure 4.13, which

depicts the amplitude of the mean Q_{10} for high and low light intensities, and the mean K_{1000} for high and low temperatures.

Temperature and light intensity had a strong, mutually dependent influence on firing and information rates. Note the dependence of the Q_{10} on light intensity and of the K_{1000} on temperature.

The coefficients of the coding efficiency and encoding window were smaller than the

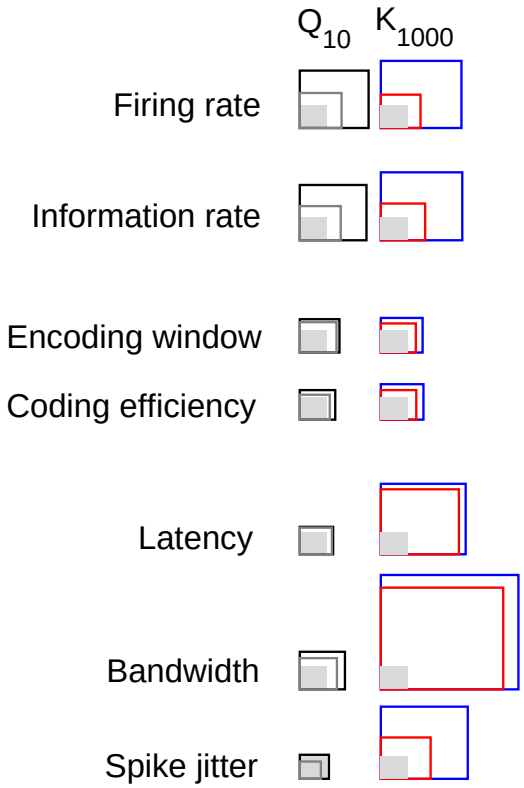

Figure 4.13: Overview of the results. The mean Q_{10} for light intensity at low light levels ($\leq$ 1 cd m^{-2}) are represented by black squares, whereas for high light levels, by gray squares. The shaded region correspond to coefficient of 1. Coefficients smaller than 1 were inverted, for sake of comparison. Similarly, the red squares represent the mean amplitudes of K_{1000} for high temperatures ($\geq$ 22°C), whereas blue squares represent the mean amplitudes for lower temperatures.

coefficients of the information rate. The K_{1000} depended more on temperature than the Q_{10} for light intensity. The variation of the K_{1000} with temperature was due mainly to the

stability of the response properties at 24 $^{\circ}C$.

Finally, for the latency, bandwidth and firing precision, the effect of the light intensity was much stronger than of temperature. The Q_{10} were not significant different from 1 for some properties at high light intensities.

Chapter 5

Discussion

Robustness is a common property of living systems. The maintenance of system performance within certain range despite internal and external perturbations usually involves trade-offs between several system properties [70]. The understanding of the principles of these processes might not only provide insight about the functionality of other robust systems but also inspire the design of new technical systems operating in random environments.

The aim of this work was to analyze how motion vision in flies changes with temperature and light intensity - two environmental characteristics that influence their visual system within the range they are behaviorally active. Focus was given on the representation of motion information.

Two principal issues were investigated in this work. The first was to determine the relative contributions of external and internal perturbations to H1 response properties. The second was to quantify to which extent the firing rate and precision influence the amount of information, coding efficiency and temporal scale of the system.

5.1 Internal and external perturbations

I demonstrated that the spike timing variability is determined mostly by the light intensity, in line with the references [9, 115, 17, 34]. Moreover, temperature does not improve H1 firing precision, contrarily to the suggestion made in ref. [198]. Thus, what determines the system variability is quality of the input signal, rather than internal noise or bandwidth - neither spontaneous events occurring throughout the system nor slower photoreceptors make motion vision less precise. However, temperature influences system reliability - H1 fails more frequently to fire spikes at low and higher temperatures than at $\approx 24^\circ$ C.

Temperature and light intensity have similar interdependent effects on the mean firing rate. Thus, firing rate robustness against thermal perturbations depends on the quality of the input signal. The Q_{10}s continuously decrease as light intensity rises - at 84 cd m^{-2}, the Q_{10} was 1.24. It is possible that the Q_{10} will remain around this value for higher light intensities, when the pupil mechanism starts to work to prevent saturation in the photoreceptors. Indeed, a previous investigation found that the effects of light intensity and temperature are not interdependent at higher light intensities [53].

5.2 Trade-off between noise and time-scale

To analyze the trade-off between temporal scale and noise, optimal encoding windows and latencies were compared with coding efficiency and standard deviation (STD) of first spike time after a particular velocity transition.

The encoding window is inversely proportional to the coding efficiency and weakly correlate with the STD (fig. 5.1). One should keep in mind that the STD reflects how precisely the stimulus can trigger a spike, but it is a local measurement. The coding efficiency on the other hand is an average measurement, but is also influenced by mean firing rate. The

latency correlates with the coding efficiency and slightly more with the STD (see also fig. 5.2). These results suggest that the more efficient and less noisy the system is, the shorter the system time-scales are.

It was shown that the latency increases dramatically when the light intensity is re-

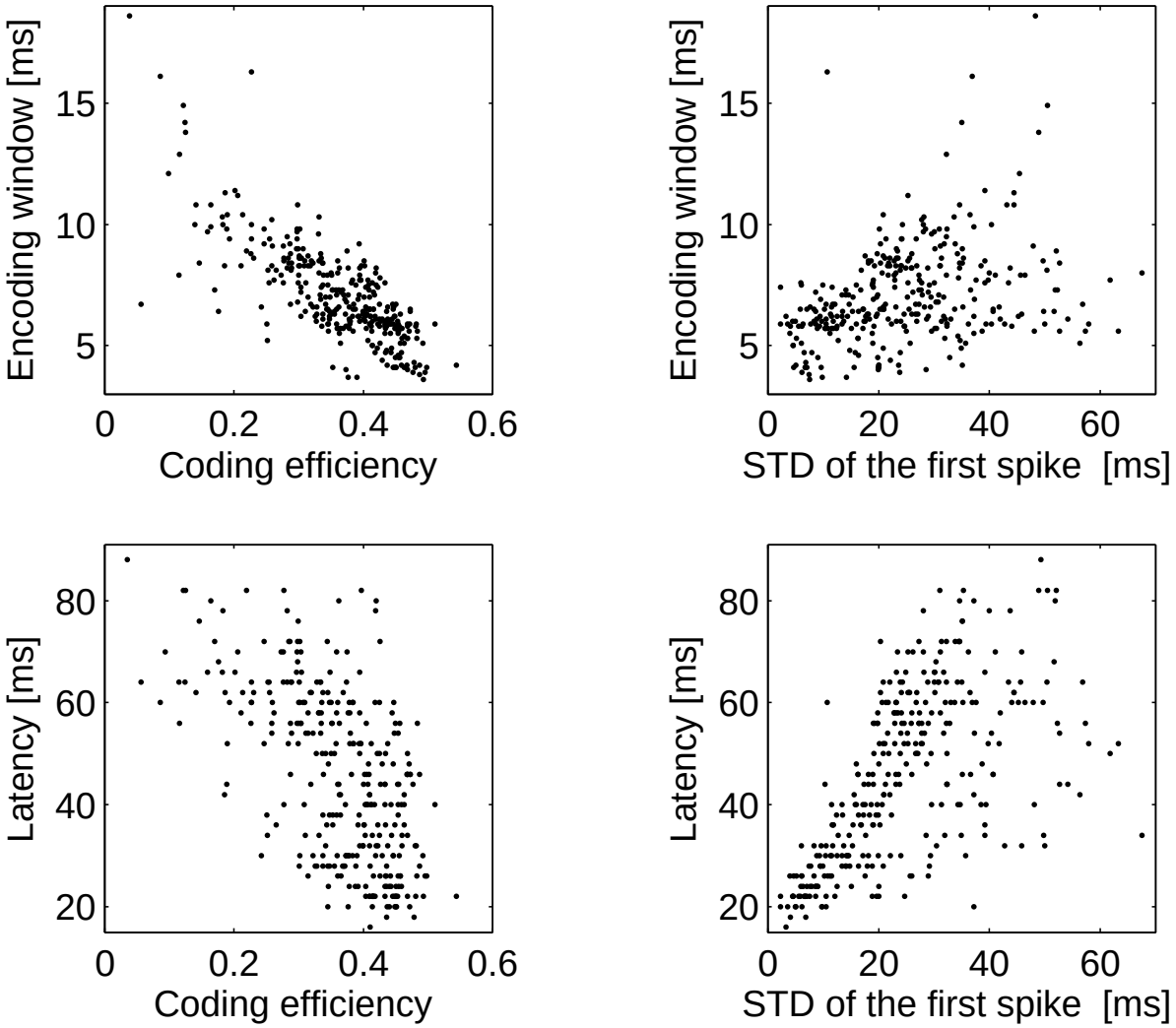

Figure 5.1: Tradeoff between the noise and temporal scale. Each point represents one acquisition. Data were pooled across temperatures and light intensities. n=325 acquisitions.

duced. It is believed that most of the response delay is due to the phototransduction cascade, since synaptic delay in flies seems to be short. However, because H1 pools the output of about several thousands of elementary motion detectors, it is possible that the

increased noise at low light intensities reduces the input synchronization in the H1 dendrites, which could increase the latency. In favor of this speculation was the fact that the latency was longer after velocity transitions, when H1 leaves its inhibited state, but was reduced after this transient period, probably because spikes that propagate back to the dendrites help to synchronize the input. If most of the latency was generated before motion computation, the observed latency in H1 response should be uniform.

To test the hypothesis that the integration process contributes to latency, flicker

Figure 5.2: Schematic showing the mutual information between response properties for the pooled data (n=325). Data was ranked before the estimation of the probability distributions. The square sizes are linearly proportional to the mutual information between the respective response properties. The biggest square represents 1.01 bit.

stimulus together with motion velocity in two different regions of the visual field were presented. It was shown that the introduction of light perturbations also increased the response latency after velocity transitions, which confirms that the noise at low light intensities generated after light transduction might be the cause of the longer latency after velocity transients. However, the flicker stimulus only increases the latency when it was

presented simultaneously with the motion stimulus, in the same region of the visual field. Simultaneously presentations of motion and flicker stimulus in separated regions did not change the response and flicker stimulus presented alone in any of the regions generated H1 responses. Altogether, the results suggest that the strong noise-dependent latency is generated during motion computation, but probably upstream H1 integration. Therefore, the hypothesis that the synchronization in the integration process influences the latency can be discarded, unless synaptic inputs outside the dendritic region where motion signal is being integrated are strongly suppressed.

5.3 Firing rate, spike jitter and information rate

The influence of spike timing variability and mean firing rate on information rate and the possible coding strategies the nervous system might use have been subject of several theoretical [119, 5, 146, 177, 68] and experimental studies [201, 164, 50, 136, 33, 151, 19, 25, 137, 3, 129] since information theory was developed [166].

These issues were also investigated in the fly's visual system. The analysis performed in this work differs from previous studies in the fly [17, 161, 83] because it examines not only the effect of firing rate and noise on information rate, but also considered the time-scale of the responses, when signal quality and system state were experimentally manipulated. My results demonstrated that the information rate is determined by the firing rate. When the input SNR increases, the strategy used by the fly seems to increase the firing rate and reduce the encoding window simultaneously.

Information and firing rates are found to be strongly correlated in other sensory systems as well. In the retina of guinea pigs, the information rates of retinal ganglion cells in response to naturalistic stimuli were more correlated with firing rate (r=0.9) than with spike jitter (r=-0.29)[104]. Also in the proprioceptive afferents in crustacean limbs, the

cross-correlation of information rate and firing rate is 0.93 whereas with spike jitter, 0.39 [42].

However, other sensory modalities make use of very precise spike times [29, 41]. For example, in the locust auditory receptors, the information rate depends on spike jitter [155]. In this study, the authors generated stimuli that elicit responses with roughly the same firing rates but different spike timing precisions. They found that the noise entropy was positive correlated with spike jitter, whereas the total entropy did not. In my results, both total and noise entropy were negative correlated with the spike jitter, which indicates that information rate was determined by the response diversity rather than spike jitter. Another difference between these two sensory modalities is the dependence of the spike timing precision with temperature - whereas H1 firing precision barely changes, an increase in temperature improves the precision of locust auditory receptors [59].

5.4 Timing and count encoding modes

The comparison between the encoding modes reveals that at time-scales where information rate was maximized, the improvement of the information rate by taking into account precise spike times within the window was around 1 bit s^{-1}, for bins of 2ms. The coding efficiency was on average 15% smaller than of the count encoding mode in these scales.

The existence of the optimum time-scales suggests that H1 conveys most of the information in the interspike intervals, as previous investigations already point out [33, 24]. Windows shorter than the optimal window convey information less efficiently because the intervals are not taken into account. On the other hand, longer windows are almost as efficient as the optimum window to represent information, but information is lost due to redundancy in the representation.

The optimum window is strongly correlated with the mode of the interspike interval

distribution (1.14 bits) (fig. 5.3) and barely correlated to mean interspike interval (0.05 bits).

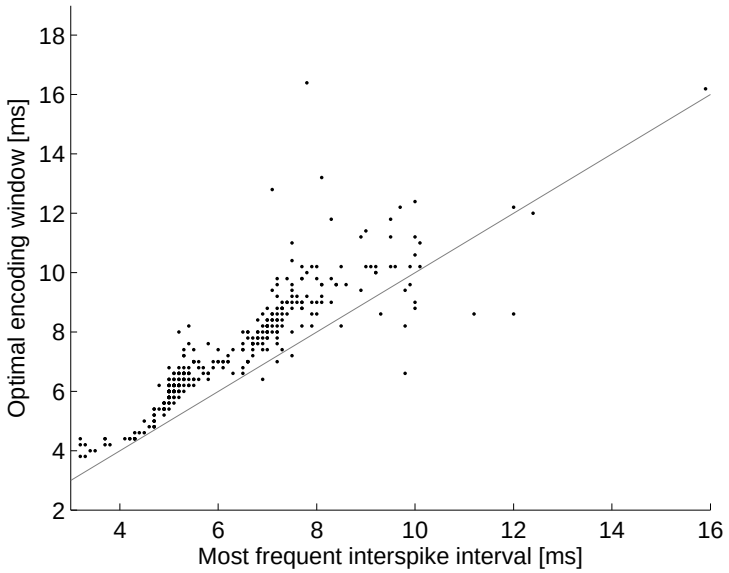

Figure 5.3: The optimal encoding window as a function of the most frequent interspike interval. n=325 acquisitions.

5.5 Behavioral relevance

The temperature range (15-27° C) used in this work covers a big part of the range that flies face at natural conditions. The light intensity range used, however, corresponds to natural light intensities of only dawn or dusk, or in internal ambients, when the photon noise becomes important. At dawn, the temperature is usually low as the light intensity increases. At dusk, the light intensity falls quickly, whereas the temperature decays slowly. Based on the results presented in this work, it can be said that the fly's visual system acquires on average the same motion information content at dawn and dusk. At dawn, however, the precision of the representation is higher than at dusk, whereas the response latency at dusk is remarkably high, despite the improved photoreceptor bandwidth that

might be provided by temperature. It is unknown to which extent optomotor latency influences the behavior of flies, but some studies reported that flies exposed to direct sunlight can be active at lower ambient temperatures than without direct exposition (see [57] and references therein).

It would be interesting to compare the flight behavior under these conditions. At least in tethered flight, it is known that the yaw torque depends on light intensity [58]. However, how the flight behavior depends on temperature is unknown. The variation of the wing beat frequency with temperature is modest - it increases 1 Hz per ° C, within a range of ambient temperatures of 13 - 30 ° C (Q_{10} of about 1.05) [188] - but it is not known whether the flight velocity and wing beat frequency are correlated, like, for example, in the smaller fly *Phaenicia sericata* [203].

It has been suggested that during flight, the increase of the head temperature due to muscle activity in the thorax would result in an improvement of the sensitivity of motion vision, matching to the high image velocities that system face during fast maneuvers [198]. However, a careful analysis of the data from reference [176] revels that, for *Calliphora* flies during tethered flight at 25°C, the head temperature increases only 2 °C (fig. 5.4). During free flight, this value might be even smaller, because convective heat loss increases. The bandwidth improvement in light adapted photoreceptors would be only 13% for an 2°C increase in temperature. For dark-adapted photoreceptors, 24%. At the highest light intensity tested here, H1's information rate would improve 4% for a 2°C increase. Thus, it seems very unlikely that *Calliphora* flies improves motion vision during flight using the heat generated in thorax - specially at high light intensities, when the photoreceptor responses are already accelerated by light-dependent mechanisms.

The situation might be different for heavier or more insulated insects [80, 123]. Heat exchange with the environment depends on several parameters [38, 30, 122], among them body surface and mass - a fly of the species *Calliphora* has a body mass of around 85mg,

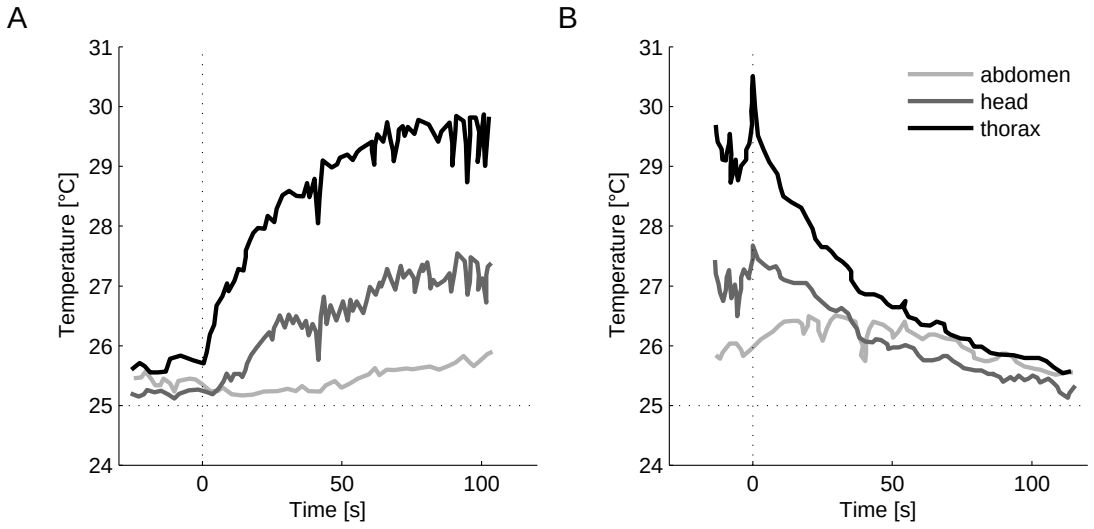

Figure 5.4: Time course of body temperature of *Calliphora* during tethered flight. **A.** Warming after start flight. **B.** Cooling after stop flight. Data reproduced from reference [176].

whereas, for example, the dragonfly *Anax junius* can weight more than one gram. The head temperature of the dragonfly can reach up to 10 °C above the ambient temperature (25°C) in still air [123], which would make sense to use the internal heat to improve vision, providing their visual systems have similar thermal sensitivities.

I showed that several response properties were stable to light intensity changes at ≈ 24 °C. Curiously, respiration (state III) in isolated mitochondria from *Calliphora* flight muscles has a maximum at ≈24-29 °C [54]. Moreover, 24 °C is preferred temperature of *Drosophila* flies [159, 71], and also the temperature at which their fitness is maximized [169]. Whether the optimal operation temperature is maintained at 24 °C when the flies are acclimated at different temperatures remains to be tested.

5.6 Conclusions and outlook

The results presented in this thesis answered a set of important questions left unanswered by the previous investigations that studied H1 neural encoding outdoors and that analyzed H1 performance as a function of temperature. It has been intensively discussed to which extent external and internal noise sources influence H1 performance. To determined the level of internal noise in the system that would be equivalent to the photon shot noise at different light intensities, I tried to vary the system intrinsic noise by controlling the temperature. For my surprise - and maybe for the reader too - I found that the thermal fluctuations in the system hardly changed H1's firing precision, despite improvement of the bandwidth of the photoreceptors [185] and considerable increase in the spontaneous activity in system. Another somewhat interesting result is the low impact of the spike timing precision in the information rate. Within the encoding window in which the information transmitted is maximized, the difference between count and timing neural encoding modes is small. Moreover, I demonstrated that the optimal encoding window varies with the environmental perturbations.

A further time-scale essential for survival, the response latency, strongly increased at low light intensities. Using stimulus flicker together with motion stimuli, I showed that noise after phototransduction might be responsible for such increased latency. The hypothesis that H1 integration process was involved in the determination of the latency remains elusive. To further investigate this problem and to determine the role of the oscillations generated in the lamina at low light intensities on H1 signal integration, it would interesting to combine the microstimulation technique [150, 190], where just a few photoreceptors are stimulated, with calcium imaging in the lobula plate [171], specially at low temperatures, when the spontaneous activity of the system is reduced.

A question left out in this work is the relation between the information transmission

and the metabolic cost. The strategy used by the fly to adjust the response to the input SNR seems to be very expensive [109] - it varies the mean firing rate. Theoretically, when the input SNR increases, it could fire the same number of spikes more precisely to better the information rate. However, I showed that by increasing the firing rate, not only the information rate is improved but also the encoding window is shortened, which is also behaviorally important. To estimate the costs of such a strategy, it would be necessary to measure the energy consumption during motion vision as a function of temperature and light intensity and relate it with the information rates - assuming that the H1 activity is proportional to the rest of the visual system during motion processing, which is somewhat reasonable, given that the H1 integrates motion information from the entire visual field.

Another problem that deserves more attention is the impact of temperature in the H1 intrinsic characteristics. The only feature measured here was the extracellular field potential, which depends also on the resistivity of the extracellular medium. It is necessary to do intracellular recordings to get access to H1 biophysical properties and relate them with the coding strategies observed. However, because of the small sizes of H1 processes, stable intracellular recordings are difficult to obtain.

The dependence of the synaptic transmission with temperature in the fly's visual system is largely unknown. The only investigation that provides such analysis measured the synaptic delay of "clock" neurons that drive some eye muscles [84]. Synapses between tangential cells in the lobula plate might be appropriate to address this problem. In addition, the system give us a good opportunity to study the thermal dependence of electrical synapses, which also can be found in the lobula plate.

Another ambitious continuation of this work would be the characterization of the impact of temperature-sensitive neurons [71] on motion information processing. For example, in the nematode *Caenorhabditis Elegans*, temperature-sensitive neurons are able to trigger the expression of heat-shock proteins in other neurons [141]. It would be interesting to

investigate whether H1 dependence on temperature would change in the absence of the corresponding temperature-sensitive neurons in fly.

Bibliography

[1] E. D. Adrian. The temperature coefficient of the refractory period in nerve. *J. Physiol. (Lond.)*, xlviii:453–464, 1914.

[2] P. Andersen and E. L. Moser. Brain temperature and hippocampal function. *hippocampus*, 5:491–498, 1995.

[3] E. Arabzadeh, S. Panzeri, and M. E. Diamond. Deciphering the spike train of a sensory neuron: Counts and temporal patterns in the rat whisker pathway. *J. Neurosci.*, 26:9216–9226, 2006.

[4] Atick. Could information theory provide an ecological theory of sensory processing? *Network*, 3:213–251, 1992.

[5] H.B. Barlow. Sensory mechanisms, the reduction of redundancy, and intelligence. In *NPL Symposium on the Mechanization of Thought Process*, number 10, pages 535–559, HM Stationery Office, London, 1959.

[6] E. F. Barrett, J. N. Barrett, D. Botz, D. B. Chang, and D. Mahaffey. Temperature-sensitive aspects of evoked and spontaneous transmitter release at frog neuromuscular junction. *J. Physiol. (Lond.)*, 279:253–273, 1978.

[7] L. Bartosch. Generation of colored noise. *Int. J. Mod. Phys. C*, 12:851–855, 2001.

[8] D. A. Baylor. Photoreceptors signals and vision. *Invest. Ophthalmol. Vis. Sci.*, 28:34–49, 1987.

[9] W. Bialek, F. Rieke, R.R. de Ruyter van Stevenick, and D. Warland. Reading a neural code. *Science*, 252:1854–1857, 1991.

[10] L. G. Bishop and D. G. Keehn. Neural correlates of the optomotor response in the fly. *Kibernetik*, 3:288–295, 1967.

[11] L.G. Bishop. Spectral response of single neurones recorded in the optic lobes of the housefly and blowfly. *Nature*, 219:1372–1373, 1968.

[12] J. Blondeau. Electrically evoked course control in the fly *Calliphora erythrocephala*. *J. Exp. Biol.*, 92:143–153, 1981.

[13] A. Borst. Noise, not stimulus entropy, determines neural information rate. *J. Comput. Neurosci.*, 14:23–31, 2003.

[14] A. Borst. Correlation versus gradient type motion detectors: the pros and cons. *Phil. Trans. R. Soc. B*, 362:369–374, 2007.

[15] A. Borst and M. Egelhaaf. Temporal modulation of luminance adapts time constant of fly movement detectors. *BioI. Cybern.*, 56:209–215, 1987.

[16] A. Borst, V. L. Flanagin, and H. Sompolinsky. Adaptation without parameter change: dynamic gain control in motion detection. *Proc. Natl. Acad. Sci. U. S. A.*, 102:6172–6176, 2005.

[17] A. Borst and J. Haag. Effects of mean firing on neural information rate. *J. Comput. Neurosci.*, 10:213–221, 2001.

[18] A. Borst and J. Haag. Neural networks in the cockpit of the fly. *J. Comp. Physiol. [A]*, 188:419–437, 2002.

[19] A. Borst and F.E. Theunissen. Information theory and neural coding. *Nat. Neurosci.*, 2:947–957, 1999.

[20] J. G. G. Borst and B. Sakmann. Effect of changes in action potential shape on calcium currents and transmitter release in a calyx-type synapse of the rat auditory brainstem. *Phil. Trans. R. Sac. Lond. B*, 354:347–355, 1999.

[21] C. B. Boschek. On the fine structure of the peripheral retina and lamina ganglionaris of the fly, *Musca domestica* . *Z. Zellforsch.*, 118:369–409, 1971.

[22] V. Braitenberg and P. Debbage. A regular net of reciprocal synapses in the visual system of the fly, *Musca domestica*. *J. Comp. Physiol.*, 90:25–31, 1974.

[23] N. Brenner, W. Bialek, and R. R. van Steveninck. Adaptive rescaling maximizes information transmission. *Neuron*, 26:695–702, 2000.

[24] N. Brenner, S.P. Strong, R. Köberle, and W. Bialek. Synergy in a neural code. *Neural Comput.*, 12:1531–1552, 2000.

[25] G. T. Buracas and T. D. Albright. Gauging sensory representations in the brain. *Trends Neurosci.*, 22:303–309, 1999.

[26] M. Burrows. Effects of temperature on a central synapse between identified motor neurons in the locust. *J. Comp. Physiol. [A]*, 165:687–695, 1989.

[27] P. A. Cariani. Temporal codes and computations for sensory representation and scene analysis. *IEEE T. Neural. Networ.*, 15:1100–1110, 2004.

[28] S. D. Carlson and C. Chi. The functional morphology of the insect photoreceptor. *Annu. Rev. Entomol.*, 24:379–416, 1979.

[29] C. E. Carr and M. A. Friedman. Evolution of time coding systems. *Neural Comput.*, 11:1–20, 1999.

[30] T. M. Casey. Biophysical ecology and heat exchange in insects. *Am. Zool.*, 332:225–237, 1992.

[31] F. S. Chance, L.F. Abbott, and A. D. Reyes. Gain modulation from background synaptic input. *Neuron*, 35:773–782, 2002.

[32] T.M. Cover and J.A. Thomas. *Elements of information theory*. John-Wiley & Sons, Inc., 1991.

[33] R. R. de Ruyter van Steveninck and W. Bialek. Real-time performance of a movement-sensitive neuron in the blowfly visual system: coding and information transfer in short spike sequences. *Proc. R. Soc. Lond. B*, 234:379–414, 1988.

[34] R. R. de Ruyter van Steveninck, A. Borst, and W. Bialek. Answerable questions and questionable answers from the fly's visual system. In M.A. All, editor, *Photoreception and Vision in Invertebrates*. 2001.

[35] R. R. de Ruyter van Steveninck and S. B. Laughlin. The rate of information transfer at graded-potential synapses. *Nature*, 379:642–645, 1996.

[36] R. R. de Ruyter van Steveninck, G.D. Lewen, S.P. Strong, R. Köberle, and W. Bialek. Reproducibility and variability in neural spike trains. *Science*, 275:1805–1808, 1997.

[37] R. R. de Ruyter van Steveninck, W. H. Zaagman, and H.A.K. Mastebroek. Adaptation of transient responses of a movement sensitive neuron in the visual system of the blowfly *Calliphora erythrocephala*. *Biol. Cybern.*, 53:451–463, 1986.

[38] W.M. Deen. *Analysis of Transport Phenomena*. Oxford University Press, New York USA, 1998.

[39] A. Destexhe, M. Rudolph, and D. Paré. The high-conductance state of neocortical neurons in vivo. *Nat. Rev. Neurosci.*, 4:379–351, 2003.

[40] R. D. DeVoe and E. M. Ockleford. Intracellular responses from cells of the medulla of the fly, *Calliphora erythrocephala*. *Biological Cybernetics*, 23:13–24, 1976.

[41] M. R. DeWeese, T. Hromádka, and A. M. Zador. Reliability and representational bandwidth in the auditory cortex. *Neuron*, 48:479–488, 2005.

[42] R.A. DiCaprio, C.R. Billimoria, and B.C. Ludwar. Information rate and spike-timing precision of proprioceptive afferents. *J Neurophysiol*, 98:1706–1717, 2007.

[43] K. A. Dill and S. Bromberg. *Molecular driving forces: statistical thermodynamics in chemistry and biology*. Garland Science, 2003.

[44] J. K. Douglass and N. J. Strausfeld. Visual motion detection circuits in flies: peripheral motion computation by identified small-field retinotopic neurons. *Journal of Neuroscience*, 15:5596–5611, 1995.

[45] J. K. Douglass, L. Wilkens, E. Pantazelou, and F. Moss. Noise enhacement of information transfer in crayfish mechanoreceptors by stochastic resonance. *Nature*, 365:337–340, 1993.

[46] R. O. Duda, P. E. Hart, and D. G. Stork. *Pattern classification*. John-Wiley & Sons, Inc., 2000.

[47] D. Dvorak, L. G. Bishop, and H. E. Eckert. On the identification of movement detectors in the fly optic lobe. *J. Comp. Physiol.*, 100:5–23, 1975.

[48] H. Eckert. Functional properties of the H1-neurone in the third optic ganglion of the blowfly, *Phaenicia*. *J. Comp. Physiol. [A]*, 135:29–39, 1980.

[49] H. Eckert. The horizontal cells in the lobula plate of the blowfly, *Phaenicia sericata*. *J. Comp. Physiol. [A]*, 143:511–526, 1981.

[50] R. Eckhorn, O.-J. Grüsser, J. Kröller, K. Pellnitz, and B. Pöpel. Efficiency of different neuronal codes: information transfer calculations for three different neuronal systems. *Biol. Cybernetics*, 22:49–60, 1976.

[51] B. Efron and G. Gong. A leisurely look at the bootstrap, the jackknife, and cross-validation. *Am. Statist.*, 37:36–48, 1983.

[52] M. Egelhaaf, A. Borst, and W. Reichardt. Computational structure of a biological motion-detection system as revealed by local detector analysis in the fly's nervous system. *J. Opt. Soc. Am. A*, 6:1070–1087, 1989.

[53] M. Egelhaaf, J. Grewe, R. Kern, and A.-K. Warzecha. Outdoor performance of a motion-sensitive neuron in the blowfly. *Vision Res.*, 41:3627–3637, 2001.

[54] R. El-Wadawi and K. Bowler. The development of thermotolerance protects blowfly flight muscle mitochondrial function from heat damage. *The Journal of Experimental Biology*, 198:2413–2421, 1995.

[55] A. L. Fairhall, G.D. Lewen, W. Bialek, and R.R. de Ruyter van Stevenick. Efficiency and ambiguity in an adaptive neural code. *Nature*, 412:787–792, 2001.

[56] A. A. Faisal, L. P. J. Selen, and D. M. Wolpert. Noise in the nervous system. *Nat. Rev. Neurosci.*, 9:292–303, 2008.

[57] J. Faucherre, D. Cherix, and C. Wyss. Behavior of *Calliphora vicina* (Diptera, Calliphoridae) under extreme conditions. *J. Insect Behav.*, 12:687–690, 1999.

[58] G. Fermi and W. Reichardt. 0ptomotorische Reaktionen der Fliege *Musca domestica*. *Kibernetik*, 2:15–28, 1963.

[59] A. Franz and B. Bonacher. Temperature dependence of temporal resolution in an insect nervous system. *J. Comp. Physiol. [A]*, 188:261–271, 2002.

[60] A. S. French. The effects of temperature on action potential encoding in the cockroach tactile spine. *J. Comp. Physiol. [A]*, 156:817–821, 1985.

[61] A. S. French and M. Järvilehto. The dynamic behavior of photoreceptor cells in the fly in response to random (white noise) stimulation at a range of temperatures. *J. Physiol. (Lond.)*, 274:311–322, 1978.

[62] G. Geiger and D. R. Nässel. Visual processing of moving single objects and wide-field patterns in flies: behavioural analysis after laser-surgical removal of interneurons. *Biol. Cybern.*, 44:141–149, 1982.

[63] J.D. Gibbons and S. Chakraborti. *Nonparametric statistical inference, fourth edition*. Marcel Dekker Inc., 2003.

[64] C. Gilbert, D. K. Penisten, and R. D. DeVoe. Discrimination of visual motion from flicker by identified neurons in the medulla of the fleshfly *Sarcophaga bullata*. *J. Comp. Physiol. [A]*, 168:653–673, 1991.

[65] J. Grewe, J. Kretzberg, A.-K. Warzecha, and M. Egelhaaf. Impact of photon noise on the reliability of a motion sensitive neuron in the fly's visual system. *J. Neurosci.*, 23:10776–10783, 2003.

[66] W. Gronenberg and N. J. Strausfeld. Descending neurons supplying the neck and flight motor of diptera: physiological and anatomical characteristics. *J. Comp. Neurol.*, 302:973–991, 1990.

[67] Y. Grossman and J. J. Kendig. Pressure and temperature: time-dependent modulation of membrane properties in a bifurcating axon. *J. Neurophysiol.*, 52:692–708, 1984.

[68] O.-J. Grüsser. Informationstheorie und die Signalverarbeitung in den Sinnesorganen und im Nervensystem. *Naturwissenschaften*, 59:436–447, 1972.

[69] Y. Gu, J. Oberwinkler, M. Postma, and R. C. Hardie. Mechanisms of light adaptation in *Drosophila* photoreceptors. *Curr. Biol.*, 15:1228–1234, 2005.

[70] H-Kitano. Biological robustness. *Nat. Rev. Genet.*, 5:826–837, 2004.

[71] F. N. Hamada, M. Rosenzweig, K. Kang, S. R. Pulver, A. Ghezzi, T. J. Jegla, and P. A. Garrity. An internal thermal sensor controlling temperature preference in *Drosophila*. *Nature*, 454:217–220, 2008.

[72] R. C. Hardie. The photoreceptor array of the dipteran retina. *Trends Neurosci.*, 9:419–423, 1986.

[73] R. C. Hardie. A histamine-activated chloride channel involved in neurotransmission at a photoreceptor synapse. *Nature*, 339:704–707, 1989.

[74] R. C. Hardie. Regulation of trp channels via lipid second messengers. *Annu. Rev. Physiol.*, 65:735–759, 2003.

[75] R.C. Hardie. Electrophysiological analysis of the fly retina. I comparative properties of R1-6 and R7 and R8. *J. Comp. Physiol. [A]*, 129:19–33, 1979.

[76] N. R. Hardingham and A. U. Larkman. The reliability of excitatory synaptic transmission in slices of rat visual cortex *in vitro* is temperature dependent. *J. Physiol. (Lond.)*, 507:249–256, 1998.

[77] K. Hausen. *Struktur, Funktion und Konnektivität bewegungempfindlicher Interneurone im dritten optischen Neuropil der Schmeissfliege Calliphora vicina*. PhD thesis, Eberhard-Karls - Universität Tübingen, 1977.

[78] K. Hausen. The lobula-complex of the fly: structure, function and significance in visual behaviour. In M.A. All, editor, *Photoreception and vision in invertebrates*. 1984.

[79] K. Hausen and C. Wehrhahn. Microsurgical lesion of horizontal cells changes optomotor yaw responses in the blowfly *Calliphora erythrocephala*. *Proc. R. Soc. Lond. B Biol. Sci.*, 219:211–216, 1983.

[80] B. Heinrich. *The Hot-blooded Insects: Strategies and Mechanisms of Thermoregulation*. Harvard University Press, Cambridge,USA, 1993.

[81] M. Heisenberg and E. Buchner. The role of retinula cell types in visual behavior of *Drosophila melanogaster*. *J. Comp. Physiol.*, 117:127–162, 1977.

[82] W. J. Heitler, C. S. Goodman, and C. H. F. Rowell. The effects of temperature on the threshold of identified neurons in the locust. *J. Comp. Physiol. [A]*, 117:163–182, 1977.

[83] J. Heitwerth, R. Kern, J. H. van Hateren, and M. Egelhaaf. Motion adaptation leads to parsimonious encoding of natural optic flow by blowfly motion vision system. *J. Neurophysiol.*, 94:1761–1769, 2005.

[84] R. Hengstenberg. Das Augenmuskelsystem der Stubenfliege *Musca domestica* 1. Analyse der "clock-spikes" und ihrer Quellen. *Kybernetik*, 2:56–77, 1971.

[85] R. Hengstenberg. Gaze control in the blowfly *Calliphora*: a multisensory, two-stage integration process. *Neurosciences*, 3:19–29, 1991.

[86] B. Hille. *Ion Channels of Excitable Membranes*. Sinauer associates, inc., Sunderland, USA, 2001.

[87] K. Hlaváčková-Schindler, M. Paluš, M. Vejmelka, and J. Bhattacharya. Causality detection based on information-theoretic approaches in time series analysis. *Physics Reports*, 441:1–46, 2007.

[88] N. Hô and A. Destexhe. Synaptic background activity enhances the responsiveness of neocortical pyramidal neurons. *J. Neurophysiol.*, 84:1488–1496, 2000.

[89] A. L. Hodgkin and B. Katz. The effect of temperature on the electrical activity of the giant axon of the squid. *J. Physiol. (Lond.)*, 109:240–249, 1949.

[90] G. R. Holt and C. Koch. Electrical interactions via the extracellular potential near cell bodies. *J. Comput. Neurosci.*, 6:169–184, 1999.

[91] J. Howard, B. Blakeslee, and S. B Laughlin. The intracellular pupil mechanism and photoreceptor signal:noise ratios in the blowfly *Lucilia cuprina*. *Proc. R. Soc. Lond. B Biol. Sci.*, 231:415–435, 1987.

[92] J. Janiszewski. The effect of temperature changes on the spontaneous activity in the neural ganglia of the cockroach, *Periplaneta americana*. *J. therm. Biol.*, 11:191–197, 1986.

[93] R. Janssen. Thermal influences on nervous system function. *Neurosci. Biobehav. Rev.*, 16:399–413, 1992.

[94] D. H. Johnson, C. M. Gruner, K. Baggerly, and C. Seshagiri. Information-theoretic analysis of neural coding. *Journal of Computational Neuroscience*, 10:47–69, 2001.

[95] M. Juusola and G. G. de Polavieja. The rate of information transfer of naturalistic stimulation by graded potentials. *J. Gen. Physiol.*, 122:191–206, 2003.

[96] M. Juusola and R. C. Hardie. Light adaptation in *Drosophila* photoreceptors: II. rising temperature increases the bandwidth of reliable signaling. *J. Gen. Physiol.*, 117:27–41, 2001.

[97] M. Juusola, E. Kouvalainen, M. Järvilehto, and M. Weckström. Contrast gain, signal-to-noise ratio, and linearity in light-adapted blowfly photoreceptors. *J. Gen. Physiol.*, 104:593–621, 1994.

[98] H. Kantz and T. Schreiber. *Nonlinear Time Series Analysis*. Cambridge University Press, Cambridge,UK, 2000.

[99] K. Kirschfeld. Die Projektion der optischen Umwelt auf das Raster der Rhabdomere im Komplexauge von *Musca*. *Exp. Brain Res.*, 3:248–270, 1967.

[100] K. Kirschfeld. Aufnahme und Verarbeitung optischer Daten im Komplexauge von Insekten. *Naturwissenschaft*, 58:201–209, 1971.

[101] K. Kirschfeld and N. Franceschini. Ein Mechanismus zur Steuerung des Lichtflusses in den Rhabdomeren des Komplexauges von *Musca*. *Kibernetik*, 6:13–22, 1969.

[102] K. Kirschfeld, N. Franceschini, and B. Minke. Evidence for a sensitising pigment in fly photoreceptors. *Nature*, 269:386–390, 1977.

[103] K. Kirschfeld and K. Vogt. Calcium ions and pigment migration in fly photoreceptors. *Naturwissenschaften*, 67:516–517, 1980.

[104] K. Koch, J. McLean, R. Segev, M. A. Freed, M. J. Berry II, V. Balasubramanian, and P. Sterling. How much the eye tells the brain. *Current Biology*, 16:1428–1434, 2006.

[105] H. G. Krapp, R. Hengstenberg, and M. Egelhaaf. Binocular contributions to optic flow processing in the fly visual system. *J. Neurophysiol.*, 85:724–734, 2001.

[106] A. Lak, E. Arabzadeh, and M. E. Diamond. Enhanced response of neurons in rat somatosensory cortex to stimuli containing temporal noise. *Cerebral Cortex*, 18:1085–1093, 2008.

[107] M. F. Land and T. S. Collett. Chasing behavior of houseflies (*Fannia canicularis*) a. description and analysis. *J. Comp. Physiol.*, 89:331–357, 1974.

[108] S. B. Laughlin. A simple coding procedure enhances a neuron's information capacity. *Z. Naturforsch. [C]*, 36c:910–912, 1981.

[109] S. B. Laughlin, R. R. de Ruyter van Stevenick, and J. C. Anderson. Metabolic cost of neural information. *Nat. Neurosci.*, 1:36–41, 1998.

[110] S. B. Laughlin and R. C. Hardie. Common strategies for light adaptation in the peripheral visual systems of fly and dragonfly. *J. Comp. Physiol. [A]*, 128:319–340, 1978.

[111] S. B. Laughlin, J.Howard, and B. Blakeslee. Synaptic limitation to contrast coding in the retina of the blowfly *Calliphora*. *Proc. R. Soc. Lond. B*, 231:437–467, 1987.

[112] S. B. Laughlin and P. G. Lillywhite. Intrinsic noise in locust photoreceptors. *J. Physiol. (Lond.)*, 332:25–45, 1982.

[113] B. P. M. Lenting, H. A. K. Mastebroek, and W. H. Zaagman. Saturation in a wide-field, directionally selective movement detection system in fly vision. *Vision Res.*, 24:1341–1347, 1984.

[114] J. E. Levin and J. P. Miller. Broadband neural encoding in the cricket cercal system enhanced by stochastic resonance. *Nature*, 380:165–168, 1996.

[115] G.D. Lewen, W. Bialek, and R. R. de Ruyter van Steveninck. Neural code of naturalistic motion stimuli. *Network: Comput. Neural Syst.*, 12:327–329, 2001.

[116] P. G. Lillywhite. The insect's compound eye. *Trends Neurosci.*, pages 169–173, 1980.

[117] P. G. Lillywhite and D. R. Dvorak. Responses to single photons in a fly optomotor neurone. *Vision Res.*, 21:279–290, 1981.

[118] H. P. Ludin and F. Beyeler. Temperature dependence of normal sensory nerve action potentials. *J. Neurol.*, 216:173–180, 1977.

[119] D. M. MacKay and W. S. McCulloch. The limiting information capacity of a neuronal link. *Bull. Math. Biophys.*, 14:127–135, 1952.

[120] T. Maddess and S. B. Laughlin. Adaptation of the motion-sensitive neuron H1 is generated locally and governed by contrast frequency. *Proc. R. Soc. Lond. B Biol. Sci.*, 225:251–275, 1985.

[121] D. G. Manolakis, V. K. Ingle, and S. M. Kogon. *Statistical and adaptive signal processing*. Artech house, 2005.

[122] M. L. May. Insect thermoregulation. *Annu. Rev. Entomol.*, 24:313–349, 1979.

[123] M. L. May. Simultaneous control of head and thoracic temperature by the green darner dragonfly *Anax Junius* (odonata: aeshnidae). *Journal of Experimental Biology*, 198:2373–2384, 1995.

[124] G. D. McCann and J. C. Dill. Fundamental properties of intensity, form, and motion perception in the visual nervous systems of *Calliphora phaenicia* and *Musca domestica*. *J. Gen. Physiol.*, 53:385–413, 1969.

[125] K. Mimura. Movement discrimination by the visual system of flies. *Z. vergl. Physiol.*, 73:105–138, 1971.

[126] B. Minke and M. Parnas. Insights on trp channels from in vivo studies in *Drosophila*. *Annu. Rev. Physiol.*, 68:649–684, 2006.

[127] T. G. A. Money, M. L. Anstey, and R. M. Robertson. Heat stress-mediated plasticity in a locust looming-sensitive visual interneuron. *J. Neurophysiol.*, 93:1908–1919, 2005.

[128] C. Montell. Visual transduction in *Drosophila*. *Annu. Rev. Cell Dev. Biol.*, 15:231–268, 1999.

[129] M.A. Montemurro, S. Panzeri, M. Maravall, A. Alenda A, M.R. Bale, M. Brambilla, and R.S. Petersen. Role of precise spike timing in coding of dynamic vibrissa stimuli in somatosensory thalamus. *J Neurophysiol*, 98:1871–1882, 2007.

[130] J. C. Montgomery and J. A. MacDonald. Effects of temperature on nervous system: implications for behavioral performance. *Am. J. Physiol.*, 259:191–196, 1990.

[131] G. P. Moore, D. H. Perkel, and J. P. Segundo. Statistical analysis and functional interpretation of neuronal spike data. *Annu. Rev. Physiol.*, 28:493–522, 1966.

[132] G. J. Murphy and F. Rieke. Network variability limits stimulus-evoked spike timing precision in retinal ganglion cells. *Neuron*, 52:511–524, 2006.

[133] P. Nordström and E. J. Warrant. Temperature-induced pupil movements in insect superposition eyes. *J. Exp. Biol.*, 203:685–692, 2000.

[134] J. C. Oberwinkler. *Calcium influx, diffusion and extrusion in fly photoreceptor cells*. PhD thesis, Rijksuniversiteit Groningen, 2000.

[135] L. M. Optican, T. J. Gawne, B. J. Richmond, and P. J. Joseph. Unbiased measures of transmitted information and channel capacity from multivariate neuronal data. *Biol. Cybern.*, 65:305–310, 1991.

[136] L. M. Optican and B. J. Richmond. Temporal encoding of two-dimensional patterns by single units in primate inferior temporal cortex. III. information theoretic analysis. *J Neurophysiol*, 57:162–178, 1987.

[137] S. Panzeri, R. S. Petersen, S. R. Schultz, M. Lebedev, and M. E. Diamond. The role of spike timing in the coding of stimulus location in rat somatosensory cortex. *Neuron*, 29:769–777, 2001.

[138] S. Panzeri, R. Senatore, M. A. Montemurro, and R.S. Petersen RS. Correcting for the sampling bias problem in spike train information measures. *J. Neurophysiol.*, 98:1064–1072, 2007.

[139] R. Plonsey and R. C. Barr. *Bioelectricity: a quantitative approach*. Springer, 2007.

[140] M. Postlethwaite, M. H. Hennig, J. R. Steinert, B. P. Graham, and I. D. Forsythe. Acceleration of ampa receptor kinetics underlies temperature-dependent changes in synaptic strength at the rat calyx of held. *Journal of physiology*, 579:69–84, 2007.

[141] V. Prahlad, T. Cornelius, and R. I. Morimoto. Regulation of the heat shock response in *Caenorhabditis elegans* by thermosensory neurons. *Science*, 320:811–814, 2008.

[142] W. H. Press, B. P. Flanney, S. A. Teukolsky, and W.T. Vetterling. *Numerical recipes in C: the art of scientific computing*. Cambridge University Press, Cambridge,UK, 1992.

[143] T. Preuss and D. S. Faber. Central cellular mechanisms underlying temperature-dependent changes in the goldfish startle-escape behavior. *J. Neurosci.*, 23:5617–5626, 2003.

[144] C. L. Prosser and D. O. Nelson. The role of nervous system in temperature adaptation of poikilotherms. *Annu. Rev. Physiol.*, 43:281–300, 1981.

[145] M. H. Quenouille. Notes on bias in estimation. *Biometrika*, 43:353–360, 1956.

[146] A. Rapoport and W. J. Horvath. The theoretical channel capacity of a single neuron as determined by various coding systems. *Information and control*, 3:335–350, 1960.

[147] W. Reichardt. Evaluation of optical motion information by movement detectors. *J. Comp. Physiol. [A]*, 161:533–547, 1987.

[148] C. Reisenman, J. Haag, and A. Borst. Adaptation of response transients in fly motion vision. I: Experiments. *Vision Res.*, 43:1291–1307, 2003.

[149] W. A. Ribi. Gap junctions coupling photoreceptor axons in the first optic ganglion of the fly. *Cell Tissue Res.*, 195:299–308, 1978.

[150] A. Riehle and N. Franceschini. Motion detection in flies: parametric control over on-off pathways. *Exp. Brain Res.*, 54:390–394, 1984.

[151] F. Rieke, D. Warland, R.R. de Ruyter van Steveninck, and W. Bialek. *Spikes-Exploring the Neural Code*. MIT Press, Cambridge,USA, 1996.

[152] H. Risken. *The Fokker-Planck equation*. Springer, 1996.

[153] J. G H. Roebroek, M. van Tjonger, and D. G. Stavenga. Temperature dependence of receptor potential an noise in fly *Calliphora erythrocephala* photoreceptor cells. *J. Insect Physiol.*, 36:499–505, 1990.

[154] J.G.H. Roebroek and D.G. Stavenga. Insect pupil mechanisms IV. spectral characteristics and light intensity dependence in the blowfly, *Calliphora erythrocephala*. *J. Comp. Physiol. [A]*, 166:537–543, 1990.

[155] A. Rokem, S. Watzl, T. Gollisch, M. Stemmler, A. V. M. Herz, and I. Samengo. Spike-timing precision underlies the coding efficiency of auditory receptor neurons. *J. Neurophysiol.*, 95:2541–2552, 2006.

[156] P. Ruoff, M. Zakhartsev, and H. V. Westerhoff. Temperature compensation through systems biology. *FEBS Journal*, 274:940–950, 2007.

[157] B. L. Sabatini and W. G. Regehr. Timing of synaptic transmission. *Annu. Rev. Physiol.*, 61:521–542, 1999.

[158] M. N. Safran, V. L. Flanagin, A. Borst, and H. Sompolinsky. Adaptation and information transmission in fly motion detection. *J. Neurophysiol.*, 98:3309–3320, 2007.

[159] O. Sayeed and S. Benzer. Behavioral genetics of thermosensation and hygrosensation in *Drosophila*. *Proc. Natl. Acad. Sci. USA*, 93:6079–6084, 1996.

[160] C. Schilstra. *Insect Flight, Eye Movements, and Vision*. PhD thesis, Rijksuniversiteit Groningen, 1999.

[161] E. Schneidman, N. Brenner, N. Tishby, R. de Ruyter van Steveninck, and W. Bialek. Universality and individuality in a neural code. In T. K. Leen, T. G. Dietterich, and V. Tresp, editors, *Advances in neural information processing systems 13*, pages 159–165. MIT Press, 2001.

[162] W. R. Schucany, H. L. Gray, and D. B. Owen. On bias reduction in estimation. *J. Am. Stat. Assoc.*, 66:524–533, 1971.

[163] F.H. Schuling, H.A.K. Mastebroek, R. Bult, and B.P.M. Lenting. Properties of elementary movement detectors in the fly *Calliphora erythrocephala*. *J. Comp. Physiol. [A]*, 165:179–192, 1989.

[164] J. P. Segundo, D. H. Perkel, and G. P. Moore. Spike probability in neurones: influence of temporal structure in the train of synaptic events. *Kibernetik*, 3:67–82, 1966.

[165] M. N. Shadlen and W. T. Newsome. The variable discharge of cortical neurons: Implications for connectivity, computation, and information coding. *J. Neurosci.*, 18:3870–3896, 1998.

[166] C.E. Shannon. A mathematical theory of communication. *Bell Sys. Tech. J.*, 27:379–423, 1948.

[167] T. O. Sharpee, H. Sugihara, A. V. Kurgansky, S. P. Rebrik, M. P. Stryker, and K. D. Miller. Adaptive filtering enhances information transmission in visual cortex. *Nature*, 439:936–942, 2006.

[168] S. R. Shaw. Early visual processing in insects. *J. exp. Biol.*, 112:225–251, 1984.

[169] W. H. Siddiqui and C. A. Barlow. Population growth of *Drosophila melanogaster* (diptera: Drosophilidae) at constant and alternating temperatures. *Annals of the Entomological Society of America*, 65:993–1001, 1972.

[170] C. L. R. Simkus and C. Stricker. Properties of mepscs recorded in layer II neurones of rat barrel cortex. *J. Physiol. (Lond.)*, 545:509–520, 2002.

[171] S. Single and A. Borst. Dendritic integration and its role in computing image velocity. *Science*, 281:1848–1850, 1998.

[172] D. P. Smith, M. A. Stamnes, and C. S. Zuker. Signal transduction in the visual system of *Drosophila*. *Annu. Rev. Cell Biol.*, 7:161–190, 1991.

[173] E. C. Smith and M. S. Lewicki. Efficient auditory coding. *Nature*, 439:978–982, 2006.

[174] D. G. Stavenga. Angular and spectral sensitivity of fly photoreceptors. I. integrated facet lens and rhabdomere optics. *J. Comp. Physiol. [A]*, 189:1–17, 2003.

[175] D. G. Stavenga. Angular and spectral sensitivity of fly photoreceptors. III. dependence on the pupil mechanism in the blowfly *Calliphora*. *J. Comp. Physiol. [A]*, 190:115–129, 2004.

[176] D. G. Stavenga, P. B. W. Schwering, and J. Tinbergen. A three-compartment model describing temperature changes in tethered flying bowflies. *J. Exp. Biol.*, 185:325–333, 1993.

[177] R. B. Stein. The information capacity of nerve cells using a frequency code. *Biophys. J.*, 7:797–826, 1967.

[178] P. J. Stephens. The effects of temperature and acclimation on crustacean nerve-muscle physiology. *Biol. Bull.*, 169:92–105, 1985.

[179] C. F. Stevens. *Neurophysiology: a primer*. John-Wiley & Sons, Inc., 1966.

[180] N. J. Strausfeld. *Facets of vision*, chapter Beneath the compound eye: neuroanatomical analysis and physiological correlates in the study of insect vision., pages 317–359. Springer, 1989.

[181] N. J. Strausfeld and J.-K. Lee. Neuronal basis for parallel visual processing in the fly. *Vis. Neurosci.*, 7:13–33, 1991.

[182] N.J. Strausfeld. *Atlas of an insect brain*. Springer, 1975.

[183] N.J. Strausfeld. Functional neuroanatomy of the blowfly's visual system. In M. A. Ali, editor, *Photoreception and Vision in Invertebrates*, page 483. Plenum, New York, 1984.

[184] S.P. Strong, R. Köberle, R.R. de Ruyter van Steveninck, and W. Bialek. Entropy and information in neural spike trains. *Phys. Rev. Lett.*, 80:197–200, 1998.

[185] B. Tatler, D. C. O'Carroll, and S. B. Laughlin. Temperature and the temporal resolving power of fly photoreceptors. *J. Comp. Physiol. [A]*, 186:399–407, 2000.

[186] F. Theunissen and J. P. Miller. Temporal encoding in nervous systems: A rigorous definition. *J. Comput. Neurosci.*, 2:149–162, 1995.

[187] P. Tiesinga, J.-M. Fellous, and T. J. Sejnowski. Regulation of spike timing in visual cortical circuits. *Nat. Rev. Neurosci.*, 9:97–109, 2008.

[188] D. M. Unwin and S. A. Corbet. Wingbeat frequency, temperature and body size in bees and flies. *Physiol. Entomol.*, 9:115–121, 1984.

[189] R. O. Uusitalo and M. Weckström. Potentiation in the first visual synapse of the fly compound eye. *J. Neurophysiol.*, 83:2103–2112, 2000.

[190] J. H. van Hateren. Neural superposition and oscillations in the eye of the blowfly. *J. Comp. Physiol. [A]*, 161:849–855, 1987.

[191] J.H. van Hateren. Electrical coupling of neuro-ommatidial photoreceptor cell in the blowfly. *J. Comp. Physiol. [A]*, 158:795–811, 1986.

[192] J.H. van Hateren. *Facets of vision*, chapter Photoreceptor optics, theory and practice., pages 74–89. Springer, 1989.

[193] J.H. van Hateren. Real and optimal neural images in early vision. *Nature*, 360:68–70, 1992.

[194] J.H. van Hateren. Processing of natural time series of intensities by the visual system of the blowfly. *Vision Res.*, 37:3407–3416, 1997.

[195] J. D. Victor. Approaches to information-theoretic analysis of neural activity. *Biological Theory*, 1:302–316, 2006.

[196] E. J. Warrant and P. D. Mcintyre. Arthropod eye design and the physical limits to spatial resolving power. *Progress in Neurobiology*, 40:413–461, 1993.

[197] A.-K. Warzecha and M. Egelhaaf. Response latency of a motion-sensitive neuron in the fly visual system: dependence on stimulus parameters and physiological conditions. *Vision Res.*, 40:2973–2983, 2000.

[198] A.-K. Warzecha, W. Horstmann, and M. Egelhaaf. Temperature-dependence of neuronal performance in the motion pathway of the bowfly *Calliphora erythrocephala*. *J. Exp. Biol.*, 202:3161–3170, 1999.

[199] M. Weckström, R. C. Hardie, and S. B. Laughlin. Voltage-activated potassium channels in blowfly photoreceptors and their role in light adaptation. *J. Physiol. (Lond.)*, 440:635–657, 1991.

[200] M. Weckström, M. Järvilehto, E. Kouvalainen, and P. Järvilehto. Fly photoreceptors and temperature: relative UV-sensitivity is increased by cooling. *Eur. Biophys. J.*, 12:173–179, 1985.

[201] G. Werner and V.B. Mountcastle. Neural activity in mechanoreceptive cutaneous afferents: stimulus-response relations, Weber functions, and information transmission. *J Neurophysiol*, 28:359–397, 1965.

[202] P.G. Willmer and D.M. Unwin. Field analyses of insect heat budgets: reflectance, size and heating rates. *Oecologia*, 50:250–255, 1981.

[203] W. J. Yurkiewicz and T. Smith. Effect of temperature on flight speed of the sheep blowfly. *J. Insect Physiol.*, 12:189–194, 1966.

[204] A. Zador. Impact of synaptic unreliability on the information transmitted by spiking neurons. *J. Neurophysiol.*, 79:1219–1229, 1998.

[205] A. M. Zoubir and B. Boashash. The bootstrap and its application in signal processing. *IEEE Signal. Proc. Mag.*, 00:56–76, 1998.

Acknowledgments

I would like to thank Prof. Alexander Borst for giving me the opportunity to work in his department, for his tolerance for my nocturnal working habits and for my quasi-obsession for perfection that almost always produced imperfect results. Without his patient, his enthusiasm and his good supervision, this work would not be finished.

I want to thank my previous advisers, Profs. Roland Köberle and Milton Ferreira de Souza for their support and guidance throughout the years.

I thank Yong Choe for enlighten discussions, his patient and generosity in helping me whenever I needed and Dierk Reiff for his wise advices.

I thank Virginia Flanagin for revealing to me the H1 secrets, for discussions and for borrowing her setup in the beginning of my PhD.

I want to thank Thomas Msric-Flogel and Werner Hemmert for being in my thesis committee and calling my attention to details which considerably contributed to the final format of this work.

I also would like to thank Yishai Elyada, Günther Zeck, Jürgen Haag, Franz Weber, Hubert Eichner, Nataly H. H. de Castro, Washington Magalhaes, Huang Wang and Alessandro Farias for many scientific discussions.

I want to thank Maximilian Joesch and Shamprasad Raghu for helping me with experiments not included in this thesis. I also thank both, and Thomas Hendel and Bettina Schnell for answering my naive questions about genetics and molecular biology. I also want to thank Thomas Hendel for his patient in listening to my practice talks.

I thank Renate Gleich for preparing the Ringer's solutions, taking care of the flies, helping me with whatever I needed in the Institute and for the Christmas cakes.

I thank also Herr Wintersberger and Herr Grass from Institute workshop for constructing part of the setup and Johannes Plett for designing and constructing the hardware for microstimulation of photoreceptors, which was however not used in the experiments reported in this thesis.

I also want to thank Christine Thalhammer and Manuela Mayer from the Institute and Maria Salgado Martinez from DAAD for their excellent advice in administrative issues.

I thank Frederich Forstner for being an extraordinary consultant for germanic issues and for helping me in many aspects.

I thank Profs. Andreas Herz, Sebastian Diehl, Elisabeth Weiss, Benedikt Grothe and Christian Leibold for their participation in the evaluation of this thesis.

I thank the DAAD and CAPES for financial support.

I also would like to thank Frederich Forstner, Maximilian Joesch, Yishai Elyada, Bernadette Rebori, Thomas Hendel and Alessandro Farias for remembering me that life is more than just science and the rest of the Borst department for providing a excellent scientific environment.

I thank my family for their understanding and unconditional support. Without them, this thesis would be feasible. This work is dedicated to the memory of my grandmother Adelia Detogni.

Versicherung

Ehrenwörtliche Versicherung:

Ich versichere hiermit ehrenwörtlich, dass ich die Dissertation mit dem Titel "The effect of temperature and light intensity on the representation of motion information in the fly's visual system" selbständig und ohne unerlaubte Beihilfe angefertigt habe. Ich habe mich dabei keiner anderen als der von mir ausdrücklich bezeichneten Hilfen und Quellen bedient.

Erklärung:

Hiermit erkläre ich, dass ich mich nicht anderweitig einer Doktorprüfung ohne Erfolg unterzogen habe. Die Dissertation wurde in ihrer jetzigen oder ähnlichen Form bei keiner anderen Hochschule eingereicht und hat noch keinen sonstigen Prüfungszwecken gedient.

München, im Oktober 2008

.....
Deusdedit Lineu Spavieri Junior

Curriculum vitae

Deusdedit Lineu Spavieri Junior

Born in Sorocaba-SP, Brazil, in 1977.
spavieri@gmx.de

EDUCATION

Max-Planck Institute of Neurobiology, Germany
Ph.D. in neurobiology
April 2005 - October 2008

University of São Paulo, São Carlos Institute of Physics, Brazil
M.Sc. in theoretical physics
August 2002 - September 2004
Grade: 4.7/5.0

University of São Paulo, São Carlos School of Engineering, Brazil
B.Sc. in electronic engineering
January 1997 - August 2002
Grade: 8.4/10.0

Stuttgart University, Germany
Undergraduate interchange student (no degree awarded)
January 2000 - March 2001

RESEARCH EXPERIENCE

Max-Planck Institute of Neurobiology
Adviser: Alexander Borst
April 2005 - October 2008
Effects of internal and external noise on motion vision.

São Carlos Institute of Physics
Adviser: Roland Köberle
August 2002 - September 2004
Information-theoretic receptive fields in the fly's visual system.

Adviser: Milton Ferreira de Souza
May 1997 - December 1999 and March 2001 - August 2002
Electrical properties of zirconia-alumina composites.

Robert Bosch GmbH, Gerlingen R&D Division, Germany
July 2000 - October 2000
Development of software of measurement systems for characterization of magnetic materials and sensors.

SCHOLARSHIPS

DAAD-CAPES PhD. October 2004 - July 2008
FAPESP M.Sc. August 2002 - September 2004
CAPES-DAAD Interchange B.Sc. January 2000 - March 2001
FAPESP B.Sc. May 1998 - December 1999 and March 2001 - August 2002

PUBLICATIONS

D.L.Spavieri Jr. and A. Borst. Effect of temperature and light intensity on motion vision. In preparation.

D.L. Spavieri Jr., L.O.B. de Almeida, J.F.W. Slaets and R. Köberle. Information-theoretic receptive fields in the fly's visual system. In preparation.

J. C. M'Peko, D. L. Spavieri Jr., C. L. da Silva, C. A. Fortulan, D. P. F. de Souza and M. F. de Souza. Electrical properties of zirconia-alumina composites,Solid State Ionics 156, 59-69, 2003.

J. C. M'Peko, D. L. Spavieri Jr. and M. F. de Souza. In situ characterization of the grain and grain boundary electrical responses of zirconia ceramics under uniaxial compressive stresses. Applied Physics Letters 81, 2827-2829, 2002.